
Robust Q-Learning against State Perturbations: a Belief-Enriched Pessimistic Approach

Anonymous Author(s)

Affiliation

Address

email

Abstract

1 Reinforcement learning (RL) has achieved phenomenal success in various domains.
2 However, its data-driven nature also introduces new vulnerabilities that can be
3 exploited by malicious opponents. Recent work shows that a well-trained RL agent
4 can be easily manipulated by strategically perturbing its state observations at the
5 test stage. Existing solutions either introduce a regularization term to improve the
6 smoothness of the trained policy against perturbations or alternatively train the
7 agent’s policy and the attacker’s policy. However, the former does not provide
8 sufficient protection against strong attacks, while the latter is computationally
9 prohibitive for large environments. In this work, we propose a new robust RL
10 algorithm for deriving a pessimistic policy to safeguard against an agent’s un-
11 certainty about true states. This approach is further enhanced with belief state
12 inference and diffusion-based state purification to reduce uncertainty. Empirical
13 results show that our approach obtains superb performance under strong attacks
14 and has a comparable training overhead with regularization-based methods.

15 1 Introduction

16 As one of the major paradigms for data-driven control, reinforcement learning (RL) provides a
17 principled and solid framework for sequential decision-making under uncertainty. However, an RL
18 agent is subject to various types of attacks, including state and reward perturbation, action space
19 manipulation, and model inference and poisoning [16]. Recent studies have shown that an RL agent
20 can be manipulated by poisoning its observation [14, 33] and reward signals [15], and a well-trained
21 RL agent can be easily defeated by a malicious opponent behaving unexpectedly [8]. In particular,
22 recent research has demonstrated the brittleness [33, 27] of existing RL algorithms in the face of
23 adversarial state perturbations, where a malicious agent strategically and stealthily perturbs the
24 observations of a trained RL agent, causing a significant loss of cumulative reward.

25 Several solutions have been proposed to combat state perturbation attacks. SA-MDP [33] imposes a
26 regularization term in the training objective to improve the smoothness of the learned policy under
27 state perturbations. This approach is improved in WocaR-RL [20] by incorporating an estimate of
28 the worst-case reward under attacks into the training objective. In a different direction, ATLA [32]
29 alternately trains the agent’s and the attacker’s policy. This approach can potentially lead to a more
30 robust policy but incurs high computational overhead, especially for large environments such as Atari
31 games with raw pixel observations.

32 Despite their promising performance in certain RL environments, the above solutions have two major
33 limitations. First, actions are directly derived from a value or policy network trained using true states,
34 despite the fact that the agent can only observe perturbed states at the test stage. This mismatch
35 between the training and testing leads to unstable performance at the test stage. Second, most existing

36 work does not exploit historical observations and the agent’s knowledge about the underlying MDP
 37 model to characterize and reduce uncertainty and infer true states in a systematic way.

38 In this work, we propose a pessimistic DQN algorithm against state perturbations by viewing the
 39 defender’s problem as finding an approximate Stackelberg equilibrium for a two-player Markov game
 40 with asymmetric observations. Given a perturbed state, the agent selects an action that maximizes the
 41 worst-case value across possible true states. This approach is applied at both training and test stages,
 42 thus removing the inconsistency between the two. We further propose two approaches to reduce
 43 the agent’s uncertainty about true states. First, the agent maintains a belief about the actual state
 44 using historical data, which, together with the pessimistic approach, provides a strong defense against
 45 large perturbations that may change the semantics of states. Second, for games with raw pixel input,
 46 such as Atari games, we train a diffusion model using the agent’s knowledge about valid states. This
 47 approach provides superb performance under commonly used attacks, with the additional advantage
 48 of being agnostic to the perturbation level. Our method achieves high robustness and significantly
 49 outperforms existing solutions under strong attacks while maintaining comparable performance under
 50 relatively weak attacks. Further, its training complexity is comparable to SA-MDP and WocaR-RL
 51 and is much lower than alternating training-based approaches.

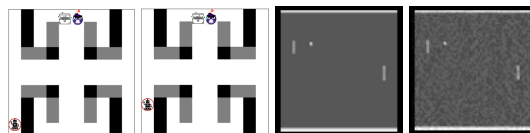
52 2 Background

53 2.1 Reinforcement Learning

54 A reinforcement learning environment is usually formulated as a Markov Decision Process (MDP),
 55 denoted by a tuple $\langle S, A, P, R, \gamma \rangle$, where S is the state space and A is the action space. $P : S \times A \rightarrow \Delta(S)$ is the transition function of the MDP, where $P(s'|s, a)$ gives the probability of
 56 moving to state s' given the current state s and action a . $R : S \times A \rightarrow \mathbb{R}$ is the reward function
 57 where $R(s, a) = \mathbb{E}(R_t | s_{t-1} = s, a_{t-1} = a)$ and R_t is the reward in time step t . Finally, γ is
 58 the discount factor. An RL agent wants to maximize its cumulative reward $G = \sum_{t=0}^T \gamma^t R_t$ over
 59 a time horizon $T \in \mathbb{Z}^+ \cup \{\infty\}$, by finding a (stationary) policy $\pi : S \rightarrow \Delta(A)$, which can be
 60 either deterministic or stochastic. For any policy π , the state-value and action-value functions
 61 are two standard ways to measure how good π is. The state-value function satisfies the Bellman
 62 equation $V_\pi(s) = \sum_{a \in A} \pi(a|s) [R(s, a) + \gamma \sum_{s' \in S} P(s'|s, a) V_\pi(s')]$ and the action-value function
 63 satisfies $Q_\pi(s, a) = R(s, a) + \gamma \sum_{s' \in S} P(s'|s, a) [\sum_{a' \in A} \pi(a'|s') Q_\pi(s', a')]$. For MDPs with a finite
 64 or countably infinite state space and a finite action space, there is a deterministic and stationary policy
 65 that is simultaneously optimal for all initial states s .
 66

67 2.2 State Adversarial Attacks in RL

68 First introduced in [14], a state perturbation attack is a test stage attack targeting an agent with
 69 a well-trained policy π . At each time step, the attacker observes the true state s_t and generates
 70 a perturbed state \tilde{s}_t (see Figure 1 for examples). The agent observes \tilde{s}_t but not s_t and takes an
 71 action a_t according to $\pi(\cdot | \tilde{s}_t)$. The attacker’s goal is to minimize the cumulative reward that
 72 the agent obtains. Note that the attacker only
 73



(a) Original (b) Perturbed (c) Original (d) Perturbed

74 The agent observes \tilde{s}_t but not s_t and takes an
 75 action a_t according to $\pi(\cdot | \tilde{s}_t)$. The attacker’s goal is to minimize the cumulative reward that
 76 the agent obtains. Note that the attacker only
 77 interferes with the agent’s observed state but not the underlying MDP. Thus, the true state in the
 78 next time step is distributed according to $P(s_{t+1} | s_t, \pi(\cdot | \tilde{s}_t))$. To limit the attacker’s capability and
 79 avoid being detected, we assume that $\tilde{s}_t \in B_\epsilon(s_t)$ where $B_\epsilon(s_t)$ is the l_p ball centered at s_t for some
 80 norm p . We consider a strong adversary that has access to both the MDP and the agent’s policy
 81 π and can perturb at every time step. With these assumptions, it is easy to see that the attacker’s
 82 problem given a fixed π can also be formulated as an MDP $\langle S, \tilde{S}, \tilde{P}, \tilde{R}, \gamma \rangle$, where both the state
 83 and action spaces are S , the transition probability $\tilde{P}(s'|s, \tilde{s}) = \sum_a \pi(a|\tilde{s}) P(s'|s, a)$, and reward
 84 $\tilde{R}(s, \tilde{s}) = - \sum_a \pi(a|\tilde{s}) R(s, a)$. Thus, an RL algorithm can be used to find a (nearly) optimal
 85 attack policy. Further, we adopt the common assumption [33, 20] that the agent has access to an
 86 intact MDP at the training stage and has access to ϵ (or an estimation of it). As we discuss below,
 87 our diffusion-based approach is agnostic to ϵ . Detailed discussions of related work on attacks and
 88 defenses in RL, including and beyond state perturbation, are in Appendix B.

89 3 Pessimistic Q-learning with State Inference and Purification

90 In this section, we give an overview of our game formu-
 91 lation and algorithmic solutions. Details can be found in
 92 Appendix C.

93 **State-Adversarial MDP as a Stackelberg Markov**
 94 **Game with Asymmetric Observations.** The problem
 95 of robust RL under adversarial state perturbations can
 96 be viewed as a two-player Markov game. The RL
 97 agent wants to find a policy $\pi : S \rightarrow \Delta(A)$ that max-
 98 imizes its long-term return, while the attacker wants
 99 to find an attack policy $\omega : S \rightarrow S$ to minimize
 100 the RL agent’s cumulative reward. The agent’s value
 101 function for a given pair of policies π and ω satis-
 102 fies the Bellman equation as $Q_{\pi \circ \omega}(s, a) = R(s, a) +$
 103 $\gamma \sum_{s' \in S} P(s'|s, a) [\sum_{a' \in A} \pi(a'|\omega(s')) Q_{\pi \circ \omega}(s', a')]$. We
 104 can consider a Stackelberg equilibrium by viewing the
 105 RL agent as the leader and the attacker as the follower to gain robustness. The agent first com-
 106 mits to a policy π . The attack observes π and identifies an optimal attack, denoted by ω_π ,
 107 as a response, where $\omega_\pi(s) = \operatorname{argmin}_{\tilde{s} \in B_\epsilon(s)} \sum_{a' \in A} \pi(a'|\tilde{s}) Q(s, a')$. Ideally, the agent wants
 108 to find a policy π^* that reaches a Stackelberg equilibrium of the game, which is defined as
 109 $\forall s \in S, \forall \pi, V_{\pi^* \circ \omega_{\pi^*}}(s) \geq V_{\pi \circ \omega_\pi}(s)$. However, previous work has shown that due to the noisy
 110 observations, finding a stationary policy that is optimal for every initial state is generally impossi-
 111 ble [33]. Thus, our goal is to find an approximate Stackelberg equilibrium, which is further improved
 112 through state prediction and denoising (see Figure 2 for the overall framework of our approach).

113 **Pessimistic Q-learning Against the Worst Case.** In this work, we present a pessimistic Q-learning
 114 algorithm (see Algorithm 1 in Appendix C.2) to address the asymmetric observations. The algorithm
 115 maintains a Q-function with the true state as the input, similar to vanilla Q-learning. But instead of
 116 using a greedy approach to derive the target policy or a ϵ -greedy approach to derive the behavior
 117 policy from the Q-function, a maximin approach is used in both cases. Figure 3 in the Appendix D
 118 illustrates the relations between a true state s , the perturbed state \tilde{s} , the worst-case state $\bar{s} \in B_\epsilon(\tilde{s})$ for
 119 which the action is chosen. In particular, it shows that the true state s must land in the ϵ -ball centered
 120 at \bar{s} , and the worst-case state the RL agent envisions is at most 2ϵ away from the true state. This gap
 121 causes performance loss that will be studied in Appendix C.6.

122 **Reducing Uncertainty Using Beliefs.** In Algorithm 1, the agent’s uncertainty against the true state
 123 is captured by the ϵ -ball around the perturbed state. The agent can utilize the sequence of historical
 124 observations and actions $\{(\tilde{s}_\tau, a_\tau)\}_{\tau < t} \cup \{\tilde{s}_t\}$ and the transition dynamics of the underlying MDP
 125 to reduce its uncertainty of the current true state s_t . To this end, we propose a simple approach to
 126 reduce the agent’s worst-case uncertainty as follows. Let $M_t \subseteq B_\epsilon(\tilde{s}_t)$ denote the agent’s belief
 127 about all possible true states at time step t . Initially, we let $M_0 = B_\epsilon(\tilde{s}_0)$. At the end of the time
 128 step t , we update the belief to include all possible next states that is reachable from the current state
 129 and action with a non-zero probability. Formally, let $M'_t = \{s' \in S : \exists s \in M_t, P(s'|s, a_t) > 0\}$.
 130 After observing the perturbed state \tilde{s}_{t+1} , we then update the belief to be the intersection of M'_t and
 131 $B_\epsilon(\tilde{s}_{t+1})$, i.e., $M_{t+1} = M'_t \cap B_\epsilon(\tilde{s}_{t+1})$, which gives the agent’s belief at time $t + 1$. When the state
 132 space is high-dimensional and continuous, computing the accurate belief is particularly hard. To deal
 133 with this, we adapt the particle filter recurrent neural network (PF-RNN) technique developed in [21]
 134 to generate belief M_t under high-dimensional state space.

135 **Purifying Invalid Observations via Diffusion.** For environments that use raw pixels as states,
 136 such as Atari Games, perturbed states generated by adding bounded noise to each pixel are mostly
 137 “invalid” in the following sense. Let $S_0 \subseteq S$ denote the set of possible initial states. Let S^0 denote
 138 the set of states that are reachable from any initial state in S_0 by following an arbitrary policy. Then
 139 perturbed states will fall outside of S^0 with high probability. This is especially the case for l_∞
 140 attacks that bound the perturbation applied to each pixel as commonly assumed in existing work
 141 (see Appendix D.2 for an example). We choose to utilize a diffusion model [12, 26] to purify the
 142 perturbed states, which obtains promising performance, as we show in our empirical results. A more
 143 detailed description of the diffusion models and our adaptations are given in Appendix B.6.

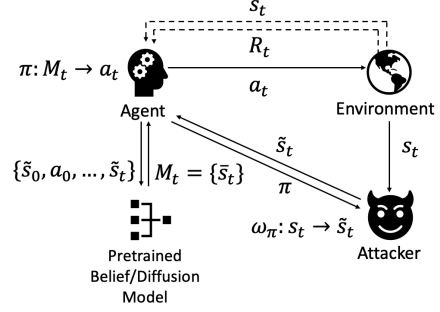


Figure 2: Belief-enriched robust RL against state perturbations. Note that the agent can only access the true state s_t and reward R_t at the training stage.

144 4 Experiments

145 We develop two pessimistic versions of the classic DQN algorithm [22] by incorporating approximate
 146 belief update and diffusion-based purification, denoted by BP-DQN and DP-DQN (see Algorithms 4-
 147 7 in Appendix F), respectively and evaluate them by conducting experiments on three environments,
 148 a continuous state Gridworld environment (shown in Figure 1a) for BP-DQN and two Atari games,
 149 Pong and Freeway for DP-DQN-O and DP-DQN-F, which utilize DDPM [12] and Progressive
 150 Distillation [26] as the diffusion model, respectively. (See Appendix G.1 for a justification.) We
 151 choose vanilla DQN [23], SA-DQN [33], and WocaR-DQN [20] as defense baselines. We consider
 152 three commonly used attacks to evaluate the robustness of these algorithms: (1) PGD attack [33];
 153 (2) MinBest attack [14]; and (3) PA-AD [27]. Details on the experiment setup can be found in
 154 Appendix G.2. Additional experiment results and ablation studies are given in Appendix G.3.

| Environment | Model | Natural Reward | PGD | | MinBest | |
|----------------------|---------------|------------------|------------------|------------------|------------------|------------------|
| | | | $\epsilon = 0.1$ | $\epsilon = 0.5$ | $\epsilon = 0.1$ | $\epsilon = 0.5$ |
| Continuous Gridworld | DQN | 156.5 \pm 90.2 | 128 \pm 118 | -53 \pm 86 | 98.2 \pm 137 | -82 \pm 20 |
| | SA-DQN | 20.8 \pm 140 | 46 \pm 142 | -100 \pm 0 | -5.8 \pm 131 | -100 \pm 0 |
| | WocaR-DQN | -100 \pm 0 | -100 \pm 0 | -63.2 \pm 88 | -100 \pm 0 | -63.2 \pm 88 |
| | BP-DQN (Ours) | 163 \pm 26 | 165 \pm 29 | 176 \pm 16 | 147 \pm 88 | 114 \pm 114 |

(a) Continuous Gridworld Results

| Env | Model | Natural Reward | PGD | | | MinBest | | | PA-AD | | |
|---------|-----------------|----------------|--------------------|--------------------|---------------------|--------------------|--------------------|---------------------|--------------------|--------------------|---------------------|
| | | | $\epsilon = 1/255$ | $\epsilon = 3/255$ | $\epsilon = 15/255$ | $\epsilon = 1/255$ | $\epsilon = 3/255$ | $\epsilon = 15/255$ | $\epsilon = 1/255$ | $\epsilon = 3/255$ | $\epsilon = 15/255$ |
| Pong | DQN | 21 \pm 0 | -21 \pm 0 | -21 \pm 0 | -21 \pm 0 | -21 \pm 0 | -21 \pm 0 | -21 \pm 0 | -18.2 \pm 2.3 | -19 \pm 2.2 | -21 \pm 0 |
| | SA-DQN | 21 \pm 0 | 21 \pm 0 | 21 \pm 0 | -20.8 \pm 0.4 | 21 \pm 0 | 21 \pm 0 | -21 \pm 0 | 21 \pm 0 | 18.7 \pm 2.6 | -20 \pm 0 |
| | WocaR-DQN | 21 \pm 0 | 21 \pm 0 | 21 \pm 0 | -21 \pm 0 | 21 \pm 0 | 21 \pm 0 | -21 \pm 0 | 21 \pm 0 | 19.7 \pm 2.4 | -21 \pm 0 |
| | DP-DQN-O (Ours) | 19.9 \pm 0.3 | 19.9 \pm 0.3 | 19.8 \pm 0.4 | 19.7 \pm 0.5 | 19.9 \pm 0.3 | 19.9 \pm 0.3 | 19.3 \pm 0.8 | 19.9 \pm 0.3 | 19.9 \pm 0.3 | 19.3 \pm 0.8 |
| | DP-DQN-F (Ours) | 21 \pm 0 | 20.4 \pm 0.7 | 20.2 \pm 0.8 | 18.6 \pm 1 | 20.2 \pm 0.9 | 19.0 \pm 0 | 19.3 \pm 1.6 | 18.0 \pm 1.0 | 17.6 \pm 1.8 | 17 \pm 2.3 |
| Freeway | DQN | 34 \pm 0.1 | 0 \pm 0 | 0 \pm 0 | 0 \pm 0 | 0 \pm 0 | 0 \pm 0 | 0 \pm 0 | 0 \pm 0 | 0 \pm 0 | 0 \pm 0 |
| | SA-DQN | 30 \pm 0 | 30 \pm 0 | 30 \pm 0 | 0 \pm 0 | 27.2 \pm 3.4 | 18.3 \pm 3.0 | 0 \pm 0 | 20.1 \pm 4.0 | 9.5 \pm 3.8 | 0 \pm 0 |
| | WocaR-DQN | 31.2 \pm 0.4 | 31.2 \pm 0.5 | 31.4 \pm 0.3 | 21.6 \pm 1 | 29.6 \pm 2.5 | 19.8 \pm 3.8 | 21.6 \pm 1 | 24.9 \pm 3.7 | 12.3 \pm 3.2 | 21.6 \pm 1 |
| | DP-DQN-O (Ours) | 28.8 \pm 1.1 | 29.1 \pm 1.1 | 29 \pm 0.9 | 28.9 \pm 0.7 | 29.2 \pm 1.0 | 28.5 \pm 1.2 | 28.6 \pm 1.3 | 28.6 \pm 1.2 | 28.3 \pm 1 | 28.8 \pm 1.3 |
| | DP-DQN-F (Ours) | 31.2 \pm 1 | 30 \pm 0.9 | 30.1 \pm 1 | 30.7 \pm 1.2 | 30.2 \pm 1.3 | 30.6 \pm 1.4 | 29.4 \pm 1.2 | 30.8 \pm 1 | 31.4 \pm 0.8 | 28.9 \pm 1.1 |

(b) Atari Games Results

Table 1: Experiment Results. We show the average episode rewards \pm standard deviation over 10 episodes for our methods and three baselines. The results for our methods are highlighted in gray.

155 4.1 Results and Discussion

156 **Continuous Gridworld.** As shown in Table 1a, our method (BP-DQN) achieves the best performance
 157 under all scenarios. In contrast, both SA-DQN and WocaR-DQN fail under the large attack budget
 158 $\epsilon = 0.5$ and perform poorly under the small attack budget $\epsilon = 0.1$. We conjecture that this is because
 159 state perturbations in the continuous Gridworld environment often change the semantics of states
 160 since most perturbed states are still valid observations. We also noticed that both SA-DQN and
 161 WocaR-DQN perform worse than vanilla DQN when there is no attack and when $\epsilon = 0.1$. We
 162 conjecture that this is due to the mismatch between true states and perturbed states during training
 163 and testing and the approximation used to estimate the upper and lower bounds of Q-network output
 164 using the Interval Bound Propagation (IBP) technique [9] in their implementations.

165 **Atari Games.** As shown in Table 1b, our DP-DQN method outperforms all other baselines under a
 166 strong attack (e.g., PA-AD) or a large attack budget (e.g., $\epsilon = 15/255$), while achieving comparable
 167 performance as other baselines in other cases. SA-DQN and WocaR-DQN fail to respond to large
 168 state perturbations for two reasons. First, both of them use IBP to estimate an upper and lower
 169 bound of the neural network output under perturbations, which are likely to be loose under large
 170 perturbations. Second, both approaches utilize a regularization-based approach to maximize the
 171 chance of choosing the best action for all states in the ϵ -ball centered at the true state. This approach
 172 is effective under small perturbations but can pick poor actions for large perturbations as the latter
 173 can easily exceed the generalization capability of the Q-network. We observe that WocaR-DQN
 174 performs better when the attack budget increases from 3/255 to 15/255 in Freeway. The reason is
 175 that under large perturbations, the agent adopts a bad policy by always moving forward regardless
 176 of state, which gives a reward of around 21. We admit that our method suffers a small performance
 177 loss compared with SA-DQN and WocaR-DQN in the Atari games when there is no attack or when
 178 the attack budget is low. We conjecture that no single fixed policy is simultaneously optimal against
 179 different types of attacks. A promising direction is to adapt a pre-trained policy to the actual attack
 180 using samples collected online.

181 References

- 182 [1] Karl J Astrom et al. Optimal control of markov processes with incomplete state information.
183 *Journal of mathematical analysis and applications*, 10(1):174–205, 1965.
- 184 [2] Dimitri P. Bertsekas and John N. Tsitsiklis. *Neuro-Dynamic Programming*. Athena Scientific,
185 1st edition, 1996.
- 186 [3] Shubham Bharti, Xuezhou Zhang, Adish Singla, and Jerry Zhu. Provable defense against
187 backdoor policies in reinforcement learning. *Advances in Neural Information Processing*
188 *Systems(NeurIPS)*, 2022.
- 189 [4] Greg Brockman, Vicki Cheung, Ludwig Pettersson, Jonas Schneider, John Schulman, Jie Tang,
190 and Wojciech Zaremba. Openai gym. *arXiv preprint arXiv:1606.01540*, 2016.
- 191 [5] Kangjie Chen, Shangwei Guo, Tianwei Zhang, Xiaofei Xie, and Yang Liu. Stealing deep
192 reinforcement learning models for fun and profit. In *Proceedings of the 2021 ACM Asia*
193 *Conference on Computer and Communications Security*, pages 307–319, 2021.
- 194 [6] Xiaoyu Chen, Yao Mark Mu, Ping Luo, Shengbo Li, and Jianyu Chen. Flow-based recurrent
195 belief state learning for pomdps. In *International Conference on Machine Learning(ICML)*,
196 2022.
- 197 [7] Tanner Fiez, Benjamin Chasnov, and Lillian Ratliff. Implicit learning dynamics in stackelberg
198 games: Equilibria characterization, convergence analysis, and empirical study. In *International*
199 *Conference on Machine Learning(ICML)*, 2020.
- 200 [8] Adam Gleave, Michael Dennis, Cody Wild, Neel Kant, Sergey Levine, and Stuart Russell.
201 Adversarial policies: Attacking deep reinforcement learning. In *International Conference on*
202 *Learning Representations(ICLR)*, 2020.
- 203 [9] Sven Gowal, Krishnamurthy Dj Dvijotham, Robert Stanforth, Rudy Bunel, Chongli Qin,
204 Jonathan Uesato, Relja Arandjelovic, Timothy Mann, and Pushmeet Kohli. Scalable verified
205 training for provably robust image classification. In *Proceedings of the IEEE/CVF International*
206 *Conference on Computer Vision*, 2019.
- 207 [10] Danijar Hafner, Timothy P Lillicrap, Mohammad Norouzi, and Jimmy Ba. Mastering atari with
208 discrete world models. In *International Conference on Learning Representations(ICLR)*, 2021.
- 209 [11] Sihong He, Songyang Han, Sanbao Su, Shuo Han, Shaofeng Zou, and Fei Miao. Robust
210 multi-agent reinforcement learning with state uncertainty. *Transactions on Machine Learning*
211 *Research*, 2023.
- 212 [12] Jonathan Ho, Ajay Jain, and Pieter Abbeel. Denoising diffusion probabilistic models. *arXiv*
213 *preprint arxiv:2006.11239*, 2020.
- 214 [13] Mengdi Huai, Jianhui Sun, Renqin Cai, Liuyi Yao, and Aidong Zhang. Malicious attacks
215 against deep reinforcement learning interpretations. In *Proceedings of the 26th ACM SIGKDD*
216 *International Conference on Knowledge Discovery & Data Mining*, pages 472–482, 2020.
- 217 [14] Sandy Huang, Nicolas Papernot, Ian Goodfellow, Yan Duan, and Pieter Abbeel. Adversarial
218 attacks on neural network policies. *arXiv:1702.02284*, 2017.
- 219 [15] Yunhan Huang and Quanyan Zhu. Deceptive reinforcement learning under adversarial manipu-
220 lations on cost signals. In *Decision and Game Theory for Security (GameSec)*, pages 217–237,
221 2019.
- 222 [16] Inaam Ilahi, Muhammad Usama, Junaid Qadir, Muhammad Umar Janjua, Ala Al-Fuqaha,
223 Dinh Thai Hoang, and Dusit Niyato. Challenges and countermeasures for adversarial attacks on
224 deep reinforcement learning. *IEEE Transactions on Artificial Intelligence*, 3(2):90–109, 2022.
- 225 [17] Ville K on onen. Asymmetric multiagent reinforcement learning. *Web Intelligence and Agent*
226 *Systems: An international journal*, 2(2):105–121, 2004.

- 227 [18] Alex X Lee, Anusha Nagabandi, Pieter Abbeel, and Sergey Levine. Stochastic latent actor-critic:
228 Deep reinforcement learning with a latent variable model. *Advances in Neural Information*
229 *Processing Systems(NeurIPS)*, 2020.
- 230 [19] Xian Yeow Lee, Sambit Ghadai, Kai Liang Tan, Chinmay Hegde, and Soumik Sarkar. Spatiotem-
231 porally constrained action space attacks on deep reinforcement learning agents. In *Proceedings*
232 *of the AAAI conference on artificial intelligence(AAAI)*, volume 34, pages 4577–4584, 2020.
- 233 [20] Yongyuan Liang, Yanchao Sun, Ruijie Zheng, and Furong Huang. Efficient adversarial training
234 without attacking: Worst-case-aware robust reinforcement learning. In *Advances in Neural*
235 *Information Processing Systems(NeurIPS)*, 2022.
- 236 [21] Xiao Ma, Péter Karkus, David Hsu, and Wee Sun Lee. Particle filter recurrent neural networks.
237 In *The Thirty-Fourth AAAI Conference on Artificial Intelligence(AAAI)*, 2020.
- 238 [22] Volodymyr Mnih, Koray Kavukcuoglu, David Silver, Alex Graves, Ioannis Antonoglou, Daan
239 Wierstra, and Martin Riedmiller. Playing atari with deep reinforcement learning, 2013.
- 240 [23] Volodymyr Mnih, Koray Kavukcuoglu, David Silver, Andrei A Rusu, Joel Veness, Marc G
241 Bellemare, Alex Graves, Martin Riedmiller, Andreas K Fidjeland, Georg Ostrovski, et al.
242 Human-level control through deep reinforcement learning. *Nature*, 518(7540):529–533, 2015.
- 243 [24] Tuomas Oikarinen, Wang Zhang, Alexandre Megretski, Luca Daniel, and Tsui-Wei Weng.
244 Robust deep reinforcement learning through adversarial loss. *Advances in Neural Information*
245 *Processing Systems(NeurIPS)*, 2021.
- 246 [25] Nicholas Roy, Geoffrey Gordon, and Sebastian Thrun. Finding approximate pomdp solutions
247 through belief compression. *Journal of artificial intelligence research*, 23:1–40, 2005.
- 248 [26] Tim Salimans and Jonathan Ho. Progressive distillation for fast sampling of diffusion models.
249 In *International Conference on Learning Representations(ICLR)*, 2022.
- 250 [27] Yanchao Sun, Ruijie Zheng, Yongyuan Liang, and Furong Huang. Who is the strongest enemy?
251 towards optimal and efficient evasion attacks in deep rl. *arXiv preprint arXiv:2106.05087*, 2021.
- 252 [28] Sebastian Tschiatschek, Kai Arulkumaran, Jan Stühmer, and Katja Hofmann. Variational
253 inference for data-efficient model learning in pomdps. *arXiv preprint arXiv:1805.09281*, 2018.
- 254 [29] Quoc-Liem Vu, Zane Alumbaugh, Ryan Ching, Quanchen Ding, Arnav Mahajan, Benjamin
255 Chasnov, Sam Burden, and Lillian J Ratliff. Stackelberg policy gradient: Evaluating the
256 performance of leaders and followers. In *ICLR 2022 Workshop on Gamification and Multiagent*
257 *Solutions*, 2022.
- 258 [30] Chaowei Xiao, Zhongzhu Chen, Kun Jin, Jiong Xiao Wang, Weili Nie, Mingyan Liu, Anima
259 Anandkumar, Bo Li, and Dawn Song. Densepure: Understanding diffusion models towards
260 adversarial robustness. *arXiv preprint arXiv:2211.00322*, 2022.
- 261 [31] Zikang Xiong, Joe Eappen, He Zhu, and Suresh Jagannathan. Defending observation attacks in
262 deep reinforcement learning via detection and denoising. Berlin, Heidelberg, 2023. Springer-
263 Verlag.
- 264 [32] Huan Zhang, Hongge Chen, Duane S Boning, and Cho-Jui Hsieh. Robust reinforcement learning
265 on state observations with learned optimal adversary. In *International Conference on Learning*
266 *Representations(ICLR)*, 2021.
- 267 [33] Huan Zhang, Hongge Chen, Chaowei Xiao, Bo Li, Mingyan Liu, Duane Boning, and Cho-
268 Jui Hsieh. Robust deep reinforcement learning against adversarial perturbations on state
269 observations. In *Advances in Neural Information Processing Systems(NeurIPS)*, 2020.
- 270 [34] Xuezhou Zhang, Yuzhe Ma, Adish Singla, and Xiaojin Zhu. Adaptive reward-poisoning attacks
271 against reinforcement learning. In *International Conference on Machine Learning(ICML)*,
272 2020.
- 273 [35] Liyuan Zheng, Tanner Fiez, Zane Alumbaugh, Benjamin Chasnov, and Lillian J Ratliff. Stack-
274 elberg actor-critic: Game-theoretic reinforcement learning algorithms. In *Proceedings of the*
275 *AAAI Conference on Artificial Intelligence(AAAI)*, 2022.

276 Appendix

277 A Broader Impacts

278 As RL is increasingly being used in vital real-world applications like autonomous driving and large
279 generative models, we are rapidly moving towards an AI-assisted society. With AI becoming more
280 widespread, it is important to ensure that the policies governing AI are robust. An unstable policy
281 could be easily exploited by malicious individuals or organizations, causing damage to property,
282 productivity, and even loss of life. Therefore, providing robustness is crucial to the successful
283 deployment of RL and other deep learning algorithms in the real world. Our work provides new
284 insights into enhancing the robustness of RL policies against adversarial attacks and contributes to
285 the foundation of trustworthy AI.

286 B Related Work

287 B.1 State Perturbation Attacks and Defenses

288 State perturbation attacks against RL policies are first introduced in [14], where the MinBest attack
289 that minimizes the probability of choosing the best action is proposed. [33] show that when the
290 agent’s policy is fixed, the problem of finding the optimal adversarial policy is also an MDP, which
291 can be solved using RL. This approach is further improved in [27], where a more efficient algorithm
292 for finding the optimal attack called PA-AD is developed.

293 On the defense side, Zhang et al. [33] prove that a policy that is optimal for any initial state under
294 optimal state perturbation might not exist and propose a set of regularization-based algorithms
295 (SA-DQN, SA-PPO, SA-DDPG) to train a robust agent against state perturbations. This approach is
296 improved in [20] by training an additional worst-case Q-network and introducing state importance
297 weights into regularization. In a different direction, an alternating training framework called ATLA
298 is studied in [32] that trains the RL attacker and RL agent alternatively in order to increase the
299 robustness of the DRL model. However, this approach suffers from high computational overhead.
300 [31] propose an auto-encoder-based detection and denoising framework to detect perturbed states and
301 restore true states. Also, [11] show that when the initial distribution is known, a policy that optimizes
302 the expected return across initial states under state perturbations exists.

303 B.2 Attacks and Defenses Beyond State Perturbations

304 This section briefly introduces other types of adversarial attacks in RL beyond state perturbation. As
305 shown in [15], manipulating the reward signal can successfully affect the training convergence of
306 Q-learning and mislead the trained agent to follow a policy that the attacker aims at. Furthermore,
307 an adaptive reward poisoning method is proposed by [34] to achieve a nefarious policy in steps
308 polynomial in state-space size $|S|$ in the tabular setting.

309 Lee et al. [19] propose two methods for perturbing the action space, where the *LAS* (look-ahead
310 action space) method achieves better attack performance in terms of decreasing the cumulative
311 reward of DRL by distributing attacks across the action and temporal dimensions. Another line of
312 work investigates adversarial policies in a multi-agent environment, where it has been shown that an
313 opponent adopting an adversarial policy could easily beat an agent with a well-trained policy in a
314 zero-sum game [8].

315 For attacking an RL agent’s policy network, both inference attacks [5], where the attacker aims
316 to steal the policy network parameters, and poisoning attacks [13] that directly manipulate model
317 parameters have been considered. In particular, an optimization-based technique for identifying an
318 optimal strategy for poisoning the policy network is proposed in [13].

319 B.3 Backdoor Attacks in RL

320 Recent work investigating defenses against backdoor attacks in RL also considers recovering true
321 states to gain robustness [3]. However, there are important differences between our work and [3].
322 First, our work contains two important parts that [3] does not have, which are the maximin formulation
323 and belief update. The former allows us to obtain a robust policy by making fewer assumptions about

324 attack behavior compared to [3]. Note that this approach is unique to state-perturbation attacks, as
 325 it is difficult to define a worst-case scenario for backdoor attacks. The latter is crucial to combat
 326 adaptive perturbations that can change the semantic meaning of states, which can potentially be very
 327 useful to backdoor attacks as well. Second, our Lipschitz assumptions differ from those in [3]. We
 328 assume that the reward and transition functions of the underlying MDP are Lipschitz continuous
 329 while [3] assume that the backdoored policies are Lipschitz continuous.

330 B.4 Partially Observable MDPs

331 As first proposed by Åström [1], a Partially Observable MDP is a generalization of an MDP where
 332 the system dynamics are determined by an MDP, but the agent does not have full access to the state.
 333 The agent could only partially observe the underlying state that is usually determined by a fixed
 334 observation function \mathcal{O} . POMDPs could model a lot of real life sequential decision-making problems
 335 such as robot navigation. However, since the agent does not have perfect information about the state,
 336 solutions for POMDPs usually need to infer a belief about the true state and find an action that is
 337 optimal for each possible belief. To this end, algorithms for finding a compressed belief space in order
 338 to solve large state space POMDPs have been proposed [25]. State-of-the-art solutions approximate
 339 the belief states with distributions such as diagonal Gaussian [18], Gaussian mixture [28], categorical
 340 distribution [10] or particle filters [21]. Most recently, a flow-based recurrent belief state modeling
 341 approach has been proposed in [6] to approximate general continuous belief states.

342 The main difference between POMDPs and MDPs under state adversarial attacks is the way the
 343 agent’s observation is determined. In a POMDP, the agent’s partial observation at time step t
 344 is determined by a fixed observation function \mathcal{O} , where $o_t = \mathcal{O}(s_t, a_t)$. And it is independent of the
 345 agent’s policy π . Instead, in an MDP under state adversarial attacks, a perturbed state \tilde{s} is determined
 346 by the attack policy ω , which can adapt to the agent’s policy π in general.

347 B.5 RL for Stackelberg Markov Games

348 Previous work has studied various techniques for solving the Stackelberg equilibrium of asymmetric
 349 Markov games, with one player as the leader and the rest being followers. Kononen [17] proposes
 350 an asymmetric multi-agent Q-Learning algorithm and establishes its convergence in the tabular
 351 setting. Besides value-based approaches, Fiez et al. [7] recently investigated sufficient conditions for
 352 a local Stackelberg equilibrium (LSE) and derived gradient-based learning dynamics for Stackelberg
 353 games using the implicit function theorem. Follow-up work applied this idea to derive Stackelberg
 354 actor-critic [35] and Stackelberg policy gradient [29] methods. However, all these studies assume
 355 that the true state information is accessible to all players, which does not apply to our problem.

356 B.6 More Details About Diffusion-Based Denoising

357 In a Denoising Diffusion Probabilistic Model (DDPM) [12], the forward process constructs a
 358 discrete-time Markov chain as follows. Given an initial state \mathbf{x}_0 sampled from $q(\cdot)$, it grad-
 359 ually adds Gaussian noise to \mathbf{x}_0 to generate a sequence of noisy states $\mathbf{x}_1, \mathbf{x}_2, \dots, \mathbf{x}_K$ where
 360 $q(\mathbf{x}_i | \mathbf{x}_{i-1}) := \mathcal{N}(\mathbf{x}_i; \sqrt{1 - \beta_i} \mathbf{x}_{i-1}, \beta_i \mathbf{I})$ so that \mathbf{x}_K approximates the Gaussian white noise.
 361 Here β_i is precalculated according to a variance schedule and \mathbf{I} is the identity matrix. The reverse
 362 process is again a Markov chain that starts with \mathbf{x}_K sampled from the Gaussian white noise $\mathcal{N}(0, \mathbf{I})$
 363 and learns to remove the noise added in the forward process to regenerate $q(\cdot)$. This is achieved
 364 through the reverse transition $p_\theta(\mathbf{x}_{i-1} | \mathbf{x}_i) := \mathcal{N}(\mathbf{x}_{i-1}; \boldsymbol{\mu}_\theta(\mathbf{x}_i, i), \boldsymbol{\Sigma}_\theta(\mathbf{x}_i, i))$ where θ denotes the
 365 network parameters used to approximate the mean and the variance added in the forward process.
 366 As mentioned in the main text, we modify the reverse process by starting from a perturbed state
 367 $\tilde{s} + \phi$ instead of \mathbf{x}_K , where ϕ is pixel-wise noise randomly sampled from range $(-\epsilon_\phi, \epsilon_\phi)$ uniformly.
 368 We then take k reverse steps with $k \ll K$, according to the observation that a perturbed state only
 369 introduces a small amount of noise to the true state due to the attack budget ϵ . We observe in our
 370 experiments that using a large k does not hurt the performance, although it increases the running time
 371 (see Figures 5d and 5e in Appendix G.3).

372 The Progressive Distillation diffusion model [26] can distill an N steps sampler to a new sampler
 373 of $N/2$ steps with little degradation of sample quality. Thus with a 1024 step sampler, we could
 374 generate 512 step, 256 step, ..., and 8 step samplers. Notice that a single reverse step in an 8 step
 375 sampler will have an equivalent effect of sampling multiple steps in the original 1024 step sampler.

376 By choosing a proper sampler generated by progressive distillation (we report every model we used
 377 in G.2), we could accelerate our diffusion process while preserving sample quality at the same time.

378 C Pessimistic Q-learning with State Inference and Purification

379 In this section, we first formulate the robust RL problem as a two-player Stackelberg Markov
 380 game. We then present our pessimistic Q-learning algorithm that derives maximin actions from
 381 the Q-function using perturbed states as the input to safeguard against the agent’s uncertainty about
 382 true states. We further incorporate a belief state approximation scheme and a diffusion-based state
 383 purification scheme into the algorithm to reduce uncertainty. Our extensions of the vanilla DQN
 384 algorithm that incorporates all three mechanisms are given in Algorithms 4-7 in Appendix F. We
 385 further give a theoretical result that characterizes the performance loss of being pessimistic.

386 C.1 State-Adversarial MDP as a Stackelberg Markov Game with Asymmetric Observations

387 The problem of robust RL under adversarial state perturbations can be viewed as a two-player Markov
 388 game, which motivates our pessimistic Q-learning algorithm given in the next subsection. The two
 389 players are the RL agent and the attacker with their state and action spaces and reward functions
 390 described in Section 2.2. The RL agent wants to find a policy $\pi : S \rightarrow \Delta(A)$ that maximizes its
 391 long-term return, while the attacker wants to find an attack policy $\omega : S \rightarrow S$ to minimize the RL
 392 agent’s cumulative reward. The game has asymmetric observations in that the attacker can observe
 393 the true states while the RL agent observes the perturbed states only. The agent’s value functions for
 394 a given pair of policies π and ω satisfy the Bellman equations below.

395 **Definition 1.** Bellman equations for state and action value functions under a state adversarial attack:
 396

$$V_{\pi \circ \omega}(s) = \sum_{a \in A} \pi(a | (\omega(s))) [R(s, a) + \gamma \sum_{s' \in S} P(s' | s, a) V_{\pi \circ \omega}(s')];$$

$$Q_{\pi \circ \omega}(s, a) = R(s, a) + \gamma \sum_{s' \in S} P(s' | s, a) [\sum_{a' \in A} \pi(a' | \omega(s')) Q_{\pi \circ \omega}(s', a')].$$

397 To achieve robustness, a common approach is to consider a Stackelberg equilibrium by viewing
 398 the RL agent as the leader and the attacker as the follower. The agent first commits to a policy
 399 π . The attack observes π and identifies an optimal attack, denoted by ω_π , as a response, where
 400 $\omega_\pi(s) = \operatorname{argmin}_{\tilde{s} \in \mathcal{B}_\epsilon(s)} \sum_{a' \in A} \pi(a' | \tilde{s}) Q(s, a')$. As the agent has access to the intact environment at
 401 the training stage and the attacker’s budget ϵ , it can, in principle, identify a robust policy proactively
 402 by simulating the attacker’s behavior. Ideally, the agent wants to find a policy π^* that reaches a
 403 Stackelberg equilibrium of the game, which is defined as follows.

404 **Definition 2.** A policy π^* is a Stackelberg equilibrium of a Markov game if

$$\forall s \in S, \forall \pi, V_{\pi^* \circ \omega_{\pi^*}}(s) \geq V_{\pi \circ \omega_\pi}(s).$$

405 A Stackelberg equilibrium ensures that the agent’s policy π^* is optimal (for any initial state) against
 406 the strongest possible *adaptive* attack and, therefore, provides a robustness guarantee. However,
 407 previous work has shown that due to the noisy observations, finding a stationary policy optimal for
 408 every initial state is generally impossible [33]. Existing solutions either introduce a regularization
 409 term to improve the smoothness of the policy or alternatively train the agent’s policy and attacker’s
 410 policy. In this paper, we take a different path with the goal of finding an approximate Stackelberg
 411 equilibrium, which is further improved through state prediction and denoising. Figure 2 shows the
 412 high-level framework of our approach, which is discussed in detail below.

413 C.2 Strategy I - Pessimistic Q-learning Against the Worst Case

414 Both value-based [17] and policy-based [35, 29] approaches have been studied to identify the
 415 Stackelberg equilibrium (or an approximation of it) of a Markov game. In particular, Stackelberg
 416 Q-learning [17] maintains separate Q-functions for the leader and the follower, which are updated by
 417 solving a stage game associated with the true state in each time step. However, these approaches do
 418 not apply to our problem as they all require both players have access to the true state in each time
 419 step. In contrast, the RL agent can only observe the perturbed state. Thus, it needs to commit to a
 420 policy for all states centered around the observed state instead of a single action, as in the stage game
 421 of Stackelberg Q-learning.

Algorithm 1: Pessimistic Q-Learning

Result: Robust Q-function Q

```
1 Initialize  $Q(s, a) = 0$  for all  $s \in S, a \in A$ ;  
2 for  $episode = 1, 2, \dots$  do  
3   Initialize true state  $s$   
4   repeat  
5     Update agent's policy:  $\forall \tilde{s} \in S, \pi(\tilde{s}) = \operatorname{argmax}_{a \in A} \min_{\bar{s} \in B_\epsilon(\tilde{s})} Q(\bar{s}, a)$ ;  
6     Update attacker's policy:  $\forall s \in S, \omega_\pi(s) = \operatorname{argmin}_{\tilde{s} \in B_\epsilon(s)} Q(s, \pi(\tilde{s}))$ ;  
7     Generate perturbed state  $\tilde{s} = \omega_\pi(s)$ ;  
8     Choose  $a$  from  $\tilde{s}$  using  $\pi$  with exploration:  
9        $a = \pi(\tilde{s})$  with probability  $1 - \epsilon'$ ; otherwise  $a$  is a random action;  
10    Take action  $a$ , observe reward  $R$  and next true state  $s'$ ;  
11    Update Q-function:  $Q(s, a) = Q(s, a) + \alpha[R(s, a) + \gamma Q(s', \pi(\omega_\pi(s'))) - Q(s, a)]$ ;  
12     $s = s'$ ;  
13  until  $s$  is terminal;  
14 end
```

422 In this work, we present a pessimistic Q-learning algorithm (see Algorithm 1) to address the above
423 challenge. The algorithm maintains a Q-function with the true state as the input, similar to vanilla
424 Q-learning. But instead of using a greedy approach to derive the target policy or a ϵ -greedy approach
425 to derive the behavior policy from the Q-function, a maximin approach is used in both cases. In
426 particular, the target policy is defined as follows (line 5). Given a perturbed state \tilde{s} , the agent picks an
427 action that maximizes the worst-case Q-value across all possible states in $B_\epsilon(\tilde{s})$, which represents
428 the agent's uncertainty. We abuse the notation a bit and let $\pi(\cdot)$ denote a deterministic policy in the
429 rest of the paper since we focus on Q-learning-based algorithms in this paper. The behavioral policy
430 is defined similarly by adding exploration (lines 8 and 9). The attacker's policy ω_π is derived as the
431 best response to the agent's policy (line 6), where a perturbed state is derived by minimizing the Q
432 value given the agent's policy.

433 A few remarks follow. First, the maximin scheme is applied when choosing an action with exploration
434 (line 9) and when updating the Q-function (line 11), and a perturbed state is used as the input in
435 both cases. In contrast, in both SA-DQN [33] and WocaR-DQN [20], actions are obtained from
436 the Q-network using true states at the training stage, while the same network is used at the test
437 stage to derive actions from perturbed states. Our approach removes this inconsistency, leading to
438 better performance, especially under relatively large perturbations. Second, instead of the pessimistic
439 approach, we may also consider maximizing the average case or the best case across $B_\epsilon(\tilde{s})$ when
440 deriving actions, which provides a different tradeoff between robustness and efficiency. Third, we
441 show how policies are derived from the Q-function to help explain the idea of the algorithm. Only
442 the Q-function needs to be maintained when implementing the algorithm.

443 Figure 3 in the Appendix D illustrates the relations between a true state s , the perturbed state \tilde{s} , the
444 worst-case state $\bar{s} \in B_\epsilon(\tilde{s})$ for which the action is chosen (line 5). In particular, it shows that the true
445 state s must land in the ϵ -ball centered at \tilde{s} , and the worst-case state the RL agent envisions is at most
446 2ϵ away from the true state. This gap causes performance loss that will be studied in Section C.6.
447 For environments with large state and action spaces, we apply the above idea to derive pessimistic
448 DQN algorithms (see Algorithms 4- 7 in Appendix F), which further incorporate state inference and
449 purification discussed below. Although we focus on value-based approaches in this work, the key
450 ideas can also be incorporated into Stackelberg policy gradient [29] and Stackelberg actor-critic [35]
451 approaches, which is left to our future work.

452 C.3 Strategy II - Reducing Uncertainty Using Beliefs

453 In Algorithm 1, the agent's uncertainty against the true state is captured by the ϵ -ball around the
454 perturbed state. A similar idea is adopted in previous regularization-based approaches [33, 20]. For
455 example, SA-MDP [33] regulates the maximum difference between the top-1 action under the true
456 state s and that under the perturbed state across all possible perturbed states in $B_\epsilon(s)$. However,
457 this approach is overly conservative and ignores the temporal correlation among consecutive states.
458 Intuitively, the agent can utilize the sequence of historical observations and actions $\{(\tilde{s}_\tau, a_\tau)\}_{\tau < t} \cup$

459 $\{\tilde{s}_t\}$ and the transition dynamics of the underlying MDP to reduce its uncertainty of the current true
 460 state s_t . This is similar to the belief state approach in partially observable MDPs (POMDPs). The
 461 key difference is that in a POMDP, the agent’s observation o_t in each time step t is derived from a
 462 fixed observation function with $o_t = O(s_t, a_t)$. In contrast, the perturbed state \tilde{s}_t is determined by
 463 the attacker’s policy ω , which is non-stationary at the training stage and is unknown to the agent at
 464 the test stage.

465 To this end, we propose a simple approach to reduce the agent’s worst-case uncertainty as follows.
 466 Let $M_t \subseteq B_\epsilon(\tilde{s}_t)$ denote the agent’s belief about all possible true states at time step t . Initially, we
 467 let $M_0 = B_\epsilon(\tilde{s}_0)$. At the end of the time step t , we update the belief to include all possible next
 468 states that is reachable from the current state and action with a non-zero probability. Formally, let
 469 $M'_t = \{s' \in S : \exists s \in M_t, P(s'|s, a_t) > 0\}$. After observing the perturbed state \tilde{s}_{t+1} , we then
 470 update the belief to be the intersection of M'_t and $B_\epsilon(\tilde{s}_{t+1})$, i.e., $M_{t+1} = M'_t \cap B_\epsilon(\tilde{s}_{t+1})$, which
 471 gives the agent’s belief at time $t + 1$. Figure 3 in the Appendix D demonstrates this process, and the
 472 formal belief update algorithm is given in Algorithm 2 in Appendix F. Our pessimistic Q-learning
 473 algorithm can easily incorporate the agent’s belief. In each time step t , instead of using $B_\epsilon(\tilde{s})$ in
 474 Algorithm 1 (line 5), the current belief M_t can be used. It is an interesting open problem to develop a
 475 strong attacker that can exploit or even manipulate the agent’s belief.

476 **Belief approximation in large state space environments.** When the state space is high-dimensional
 477 and continuous, computing the accurate belief as described above becomes infeasible as computing
 478 the intersection between high-dimensional spaces is particularly hard. Previous studies have proposed
 479 various techniques to approximate the agent’s belief about true states using historical data in partially
 480 observable settings, including using classical RNN networks [21] and flow-based recurrent belief
 481 state learning [6]. In this work, we adapt the particle filter recurrent neural network (PF-RNN)
 482 technique developed in [21] to our setting due to its simplicity. In contrast to a standard RNN-based
 483 belief model $B : (S \times A)^t \rightarrow H$ that maps the historical observations and actions to a deterministic
 484 latent state h_t , PF-RNN approximates the belief $b(h_t)$ by κ_p weighted particles in parallel, which are
 485 updated using the particle filter algorithm according to the Bayes rule. An output function f_{out} then
 486 maps the weighted average of these particles in the latent space to a prediction of the true state in the
 487 original state space.

488 To apply PF-RNN to our problem, we first train the RNN-based belief model N and the prediction
 489 function f_{out} before learning a robust RL policy. This is achieved by using C trajectories generated
 490 by a random agent policy and a random attack policy in an intact environment. Then at each time
 491 step t during the RL training and testing, we use the belief model N and historical observations and
 492 actions to generate κ_p particles, map each of them to a state prediction using f_{out} , and take the set of
 493 κ_p predicted states as the belief M_t about the true state. PF-RNN includes two versions that support
 494 LSTM and GRU, respectively, and we use PF-LSTM to implement our approach. We define the
 495 complete belief model utilizing PF-RNN as $N_p \triangleq f_{out} \circ B$.

496 We remark that previous work has also utilized historical data to improve robustness. For example,
 497 [31] uses an LSTM-autoencoder to detect and denoise abnormal states at the test stage, and [32] con-
 498 sideres an LSTM-based policy in alternating training. However, none of them explicitly approximate
 499 the agent’s belief about true states and use it to derive a robust policy.

500 C.4 Strategy III - Purifying Invalid Observations via Diffusion

501 For environments that use raw pixels as states, such as Atari Games, perturbed states generated by
 502 adding bounded noise to each pixel are mostly “invalid” in the following sense. Let $S_0 \subseteq S$ denote
 503 the set of possible initial states. Let S^0 denote the set of states that are reachable from any initial
 504 state in S_0 by following an arbitrary policy. Then perturbed states will fall outside of S^0 with high
 505 probability. This is especially the case for l_∞ attacks that bound the perturbation applied to each
 506 pixel as commonly assumed in existing work (see Appendix D.2 for an example). This observation
 507 points to a fundamental limitation of existing perturbation attacks that can be utilized by an RL agent
 508 to develop a more efficient defense.

509 One way to exploit the above observation is to identify a set of “valid” states near a perturbed state
 510 and use that as the belief of the true state. However, it is often difficult to check if a state is valid
 511 or not and to find such a set due to the fact that raw pixel inputs are usually high-dimensional.

512 Instead, we choose to utilize a diffusion model to purify the perturbed states, which obtains promising
 513 performance, as we show in our empirical results.

514 To this end, we first sample C' trajectories from a clean environment using a pre-trained policy
 515 without attack to estimate a state distribution $q(\cdot)$, which is then used to train a Denoising Diffusion
 516 Probabilistic Model (DDPM) [12]. Then during both RL training and testing, when the agent receives
 517 a perturbed state \tilde{s} , it applies the reverse process of the diffusion model for k steps to generate a set of
 518 purified states as the belief M_t of size κ_d , where k and κ_d are hyperparameters. We let $N_d : S \rightarrow S^{\kappa_d}$
 519 denote a diffusion-based belief model. Note that rather than starting from random noise in the reverse
 520 process as in image generation, we start from a perturbed state that the agent receives and manually
 521 add a small amount of pixel-wise noise ϕ to it before denoising, inspired by denoised smoothing
 522 in deep learning [30]. We observe in experiments that using a large k does not hurt performance,
 523 although it increases the running time. Thus, unlike previous work, this approach is agnostic to
 524 the accurate knowledge of attack budget ϵ . One problem with DDPM, however, is that it incurs
 525 high overhead to train the diffusion model and sample from it, making it less suitable for real-time
 526 decision-making. To this end, we further evaluate a recently developed fast diffusion technique,
 527 Progressive Distillation [26], which distills a multi-step sampler into a few-step sampler. As we
 528 show in the experiments, the two diffusion models provide different tradeoffs between robustness and
 529 running time. A more detailed description of the diffusion models and our adaptations are given in
 530 Appendix B.6.

531 C.5 Pessimistic DQN with Approximate Beliefs and State Purification

532 Built upon the above ideas, we develop two pessimistic versions of the classic DQN algorithm [22]
 533 by incorporating approximate belief update and diffusion-based purification, denoted by BP-DQN
 534 and DP-DQN, respectively. The details are provided in Algorithms 4- 7 in Appendix F. Below we
 535 highlight the main differences between our algorithms and vanilla DQN.

536 The biggest difference lies in the loss function, where we incorporate the maximin search into the
 537 loss function to target the worst case. Concretely, instead of setting $y_i = R_i + \gamma \max_{a' \in A} Q'(s_i, a')$
 538 as in vanilla DQN, we set $y_i = R_i + \gamma \max_{a' \in A} \min_{m \in M_i} Q'(m, a')$ where R_i, s_i, M_i are sampled
 539 from the replay buffer and Q' is the target network. Similarly, instead of generating actions using the
 540 ϵ -greedy (during training) or greedy approaches (during testing), the maximin search is adopted.

541 To simulate the attacker’s behavior, one needs to identify the perturbed state \tilde{s} that minimizes the
 542 Q value under the current policy π subject to the perturbation constraint. As finding the optimal
 543 attack under a large state space is infeasible, we solve the attacker’s problem using projected gradient
 544 descent (PGD) with η iterations to find an approximate attack similar to the PGD attack in [33]. In
 545 BP-DQN where approximate beliefs are used, the history of states and actions is saved to generate
 546 the belief in each round. In DP-DQN where diffusion is used, the reverse process is applied to both
 547 perturbed and true states. That is, the algorithm keeps the purified version of the true states instead of
 548 the original states in the replay buffer during training. We find this approach helps reduce the gap
 549 between purified states and true states. In both cases, instead of training a robust policy from scratch,
 550 we find that it helps to start with a pre-trained model obtained from an attack-free MDP.

551 We want to highlight that BP-DQN is primarily designed for environments with structural input,
 552 whereas DP-DQN is better suited for environments with raw pixel input. Both approaches demonstrate
 553 exceptional performance in their respective scenarios, even when faced with strong attacks, as shown
 554 in our experiments. Thus, although combining the two methods by integrating history-based belief
 555 and diffusion techniques may seem intuitive, this is only needed when confronted with an even more
 556 formidable attacker, such as one that alters both semantic and pixel information in Atari games.

557 C.6 Bounding Performance Loss due to Pessimism

558 In this section, we characterize the impact of being pessimistic in selecting actions. To obtain insights,
 559 we choose to work on a pessimistic version of the classic value iteration algorithm (see Algorithm 3
 560 in Appendix F), which is easier to analyze than the Q-learning algorithm presented in Algorithm 1.
 561 To this end, we first define the Bellman operator for a given pair of policies.

562 **Definition 3.** For a given pair of agent policy π and attack policy ω , the Bellman operator for the
 563 Q-function is defined as follows.

$$T^{\pi \circ \omega} Q(s, a) = R(s, a) + \gamma \sum_{s' \in S} P(s' | s, a) Q(s', \pi(\omega(s'))) \quad (1)$$

564 The algorithm maintains a Q-function, which is initialized to 0 for all state-action pairs. In each
 565 round n , the algorithm first derives the agent’s policy π_n and attacker’s policy ω_{π_n} from the current
 566 Q-function Q_n in the same way as in Algorithm 1, using the worst-case belief, where

$$\begin{aligned}\pi_n(\tilde{s}) &= \operatorname{argmax}_{a \in A} \min_{\bar{s} \in B_\epsilon(\tilde{s})} Q_n(\bar{s}, a), \forall \tilde{s} \in S. \\ \omega_{\pi_n}(s) &= \operatorname{argmin}_{\bar{s} \in B_\epsilon(s)} Q_n(s, \pi_n(\bar{s})), \forall s \in S.\end{aligned}$$

567 That is, π_n is obtained by solving a maximin problem using the current Q_n , and ω_{π_n} is a best
 568 response to π_n . The Q-function is then updated as $Q_{n+1} = T^{\pi_n \circ \omega_{\pi_n}} Q_n$. It is important to note that
 569 although $T^{\pi \circ \omega_\pi}$ is a contraction for a fixed π (see Lemma 3 in Appendix E for a proof), $T^{\pi_n \circ \omega_{\pi_n}}$ is
 570 typically not due its dependence on Q_n . Thus, Q_n may not converge in general, which is consistent
 571 with the known fact that a state-adversarial MDP may not have a stationary policy that is optimal for
 572 every initial state. However, we show below that we can still bound the gap between the Q-value
 573 obtained by following the joint policy $\tilde{\pi}_n := \pi_n \circ \omega_{\pi_n}$, denoted by $Q^{\tilde{\pi}_n}$, and the optimal Q-value for
 574 the original MDP without attacks, denoted by Q^* . It is known that Q^* is the unique fixed point of the
 575 Bellman optimal operator T^* , i.e., $T^*Q^* = Q^*$, where

$$T^*Q(s, a) = R(s, a) + \gamma \sum_{s' \in S} P(s'|s, a) \max_{a' \in A} Q(s', a'). \quad (2)$$

576 We first make the following assumptions about the reward and transition functions of an MDP and
 577 then state the main result after that.

578 **Assumption 1.** The reward function and transition function are Lipschitz continuous. That is, there
 579 are constants l_r and l_p such that for $\forall s_1, s_2, s' \in S, \forall a \in A$, we have

$$|R(s_1, a) - R(s_2, a)| \leq l_r \|s_1 - s_2\|, |P(s'|s_1, a) - P(s'|s_2, a)| \leq l_p \|s_1 - s_2\|.$$

580 **Assumption 2.** Reward R is upper bounded where for any $s \in S$ and $a \in A$, $R(s, a) \leq R_{max}$.

582 **Theorem 1.** *The gap between $Q^{\tilde{\pi}_n}$ and Q^* is bounded by*

$$\limsup_{n \rightarrow \infty} \|Q^* - Q^{\tilde{\pi}_n}\|_\infty \leq \frac{1 + \gamma}{(1 - \gamma)^2} \Delta,$$

583 where $\tilde{\pi}_n$ is obtained by Algorithm 3 and $\Delta = 2\epsilon\gamma(l_r + l_p|S| \frac{R_{max}}{1-\gamma})$.

584 We give a proof sketch and leave the detailed proof in Appendix E. We first show that $Q^{\tilde{\pi}_n}$ is Lipschitz
 585 continuous using Assumption 1. Then we establish a bound of $\|T^*Q_n - Q_{n+1}\|_\infty$ and prove that
 586 $T^{\pi \circ \omega_\pi}$ for a fixed policy π is a contraction. Finally, we prove Theorem 1 following the idea of
 587 Proposition 6.1 in [2].

588 D More Graphs and Examples

589 D.1 An Example of Belief Update

590 Figure 3 illustrates the relations between a true state s , the perturbed state \tilde{s} , and the worst-case state
 591 $\bar{s} \in B_\epsilon(\tilde{s})$ for which the action is chosen.

592 D.2 An Example of Invalid States in Pixel-wise Perturbations

593 For example, the white bar shown in Figure 4 in Atari Pong game will not change during game
 594 play and has grayscale value of 236/255. However, a pixel wise state perturbation attack such
 595 as PGD with attack budget $\epsilon = 15/255$ will change the pixel values in the white bar to range of
 596 221/255 – 251/255 so that the perturbed states become invalid.

597 E Proofs

598 E.1 Proof of Theorem 1

599 In this section, we prove Theorem 1. Recall that $\tilde{\pi} := \pi \circ \omega_\pi$. We first establish the Lipschitz continuity
 600 of $Q^{\tilde{\pi}}$, the Q-value when the agent follows policy π and the attack follows policy ω_π .

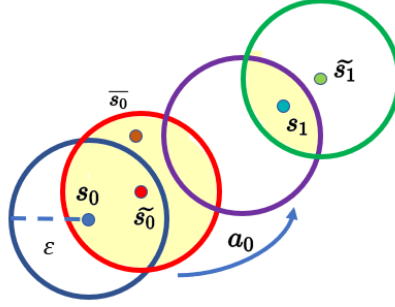


Figure 3: True, perturbed, and worst-case states in Algorithm 1 and belief update. Beginning with true state s_0 and perturbed state \tilde{s}_0 , the agent will have an initial belief, i.e., the ϵ ball centered at \tilde{s}_0 . After taking action a_0 , the belief is updated to the region marked by the purple ball. When observing the next perturbed state \tilde{s}_1 , the agent will update belief by taking the intersection of the purple ball and the green ball.

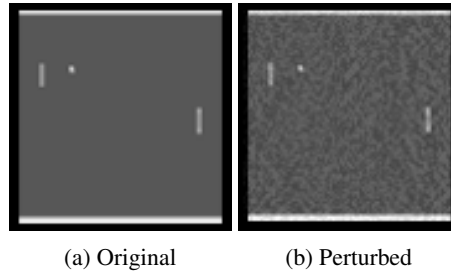


Figure 4: An example of valid vs. invalid states in Pong.

601 **Lemma 1.** $Q^{\tilde{\pi}}$ is Lipchitz continuous for any π , i.e., $\forall s, s' \in S, \forall a \in A$,

$$|Q^{\tilde{\pi}}(s, a) - Q^{\tilde{\pi}}(s', a)| \leq \mathcal{L}_{Q_f} \|s - s'\| \quad (3)$$

602 where $L_{Q_f} = l_r + \frac{R_{max}}{1-\gamma} |S| l_p$

603 *Proof.* Based on the definition of the action value function under state perturbation, we have

604

$$\begin{aligned} Q^{\tilde{\pi}}(s, a) &= R(s, a) + \sum_{s' \in S} P(s'|s, a) \gamma V_{\pi \circ \omega_{\pi}}(s') \\ &\leq R(s, a) + \sum_{s' \in S} P(s'|s, a) \gamma V_{\pi}(s') \end{aligned}$$

605 Thus,

$$\begin{aligned} &|Q^{\tilde{\pi}}(s_1, a) - Q^{\tilde{\pi}}(s_2, a)| \\ &= |R(s_1, a) - R(s_2, a) + \sum_{s' \in S} [(P(s'|s_1, a) - P(s'|s_2, a)) V_{\pi \circ \omega_{\pi}}(s')]| \\ &\leq |R(s_1, a) - R(s_2, a)| + \sum_{s' \in S} |(P(s'|s_1, a) - P(s'|s_2, a)) V_{\pi}(s')| \\ &\stackrel{(a)}{\leq} l_r \|s_1 - s_2\| + \max_{s' \in S} V_{\pi}(s') |S| |P(s'|s_1, a) - P(s'|s_2, a)| \\ &\stackrel{(b)}{\leq} l_r \|s_1 - s_2\| + \frac{R_{max}}{1-\gamma} |S| l_p \|s_1 - s_2\| \\ &\leq (l_r + \frac{R_{max}}{1-\gamma} |S| l_p) \|s_1 - s_2\| \\ &= \mathcal{L}_{Q_f} \|s_1 - s_2\| \end{aligned}$$

606 where (a) follows from Assumption 1 and (b) follows from Assumptions 1 and 2 and the definition of
607 V_{π} . \square

608 **Lemma 2.** For Q_n defined in Algorithm 3, the Bellman approximation error is bounded by

$$\|T^* Q_n - Q_{n+1}\|_{\infty} \leq 2\epsilon \gamma (l_r + l_p) |S| \frac{R_{max}}{1-\gamma} \quad (4)$$

Proof.

$$\begin{aligned}
& \|T^*Q_n - Q_{n+1}\|_\infty \\
&= \max_{s \in S, a \in A} |R(s, a) + \gamma \sum_{s'} P(s'|s, a) \max_{a \in A} Q_n(s', a) - [R(s, a) + \gamma \sum_{s'} P(s'|s, a) Q_n(s', \pi_n(\omega_{\pi_n}(s')))]| \\
&= \gamma \max_{s \in S, a \in A, s' \in S} \sum_{s' \in S} P(s'|s, a) |\max_{a \in A} Q_n(s', a) - Q_n(s', \tilde{\pi}_n(s'))| \\
&\leq \gamma \max_{s' \in S} |\max_{a \in A} Q_n(s', a) - Q_n(s', \tilde{\pi}_n(s'))|
\end{aligned}$$

609 Let $\tilde{s}' = \omega_{\pi_n}(s')$ denote the perturbation of the true state s' , and \tilde{a} and \tilde{s}' denote the agent's action
610 when observing \tilde{s}' and the worst-case state in $B_\epsilon(\tilde{s}')$ that solves the maximin problem, respectively.
611 We then have

$$Q_n(s', \tilde{a}) \geq Q_n(\tilde{s}', \tilde{a}) = \max_{a \in A} \min_{s \in B_\epsilon(\tilde{s}')} Q_n(s, a). \quad (5)$$

612 where the first inequality is due to the fact that \tilde{s}' obtains the worst-case Q-value under action \tilde{a} ,
613 across all states in $B_\epsilon(\tilde{s}')$ including s' . It follows that

$$\begin{aligned}
\|T^*Q_n - Q_{n+1}\|_\infty &\leq \gamma \max_{s' \in S} |\max_{a \in A} Q_n(s', a) - Q_n(s', \tilde{\pi}(s'))| \\
&\leq \gamma \max_{s' \in S} |\max_{a \in A} Q_n(s', a) - \max_{a \in A} \min_{s \in B_\epsilon(\tilde{s}')} Q_n(s, a)| \\
&\leq \gamma \max_{s' \in S, a \in A} |Q_n(s', a) - \min_{s \in B_\epsilon(\tilde{s}')} Q_n(s, a)| \\
&\stackrel{(a)}{\leq} \gamma \max_{s' \in S, a \in A} |Q_n(s', a) - \min_{s \in B_{2\epsilon}(s')} Q_n(s, a)| \\
&\stackrel{(b)}{\leq} 2\gamma \epsilon \mathcal{L}_{Q_f}
\end{aligned}$$

614 where (a) is due to $\|\tilde{s}' - s'\| \leq \epsilon$ and (b) follows from Lemma 1. □

615 **Lemma 3.** *Given any policy $\tilde{\pi} = \pi \circ \omega_\pi$ where π is a fixed policy, $T^{\tilde{\pi}}$ is a contraction.*

Proof.

$$\begin{aligned}
\|T^{\tilde{\pi}}Q_1 - T^{\tilde{\pi}}Q_2\|_\infty &= \max_{s \in S, a \in A, s' \in S} \sum_{s' \in S} \gamma P(s'|s, a) |Q_1(s', \pi(\omega(s'))) - Q_2(s', \pi(\omega(s')))| \\
&\leq \max_{s' \in S} \gamma |Q_1(s', \pi(\omega(s'))) - Q_2(s', \pi(\omega(s')))| \\
&\leq \max_{s' \in S, a \in A} \gamma |Q_1(s', a) - Q_2(s', a)| \\
&= \gamma \|Q_1 - Q_2\|_\infty
\end{aligned}$$

616 Thus, for any given policy π , $T^{\tilde{\pi}}$ is a contraction. □

617 With Lemmas 2 and 3, we are ready to prove Theorem 1.

618 **Theorem 1.** *The gap between $Q^{\tilde{\pi}_n}$ and Q^* is bounded by*

619

$$\limsup_{n \rightarrow \infty} \|Q^* - Q^{\tilde{\pi}_n}\|_\infty \leq \frac{1 + \gamma}{(1 - \gamma)^2} \Delta$$

620 where $\tilde{\pi}_n$ is obtained by Algorithm 3 and $\Delta = 2\epsilon\gamma(l_r + l_p|S|^{\frac{R_{\max}}{1-\gamma}})$.

Proof.

$$\begin{aligned}
\|Q^* - Q^{\tilde{\pi}_n}\|_\infty &\stackrel{(a)}{\leq} \|T^*Q^* - T^*Q_n\|_\infty + \|T^*Q_n - T^{\tilde{\pi}_n}Q^{\tilde{\pi}_n}\|_\infty \\
&\leq \|T^*Q^* - T^*Q_n\|_\infty + \|T^*Q_n - T^{\tilde{\pi}_n}Q_n\|_\infty + \|T^{\tilde{\pi}_n}Q_n - T^{\tilde{\pi}_n}Q^{\tilde{\pi}_n}\|_\infty \\
&\stackrel{(b)}{\leq} \gamma \|Q^* - Q_n\|_\infty + \|T^*Q_n - Q_{n+1}\|_\infty + \gamma (\|Q_n - Q^*\|_\infty + \|Q^* - Q^{\tilde{\pi}_n}\|_\infty)
\end{aligned}$$

| Q_1 | s_1 | s_2 | s_3 | Q_2 | s_1 | s_2 | s_3 |
|-------|-------|-------|-------|-------|-------|-------|-------|
| a_1 | 12 | 11 | 3 | a_1 | 4 | 2 | -2 |
| a_2 | 12 | 10 | 2 | a_2 | 4 | 0 | -1 |
| a_3 | 12 | 8 | 1 | a_3 | 4 | 1 | -3 |

Table 2: A counterexample to $T^{\pi_n \circ \omega_{\pi_n}}$ being a contraction

621 where (a) follows from Q^* is the fixed point of T^* , $Q^{\tilde{\pi}_n}$ is the fixed point of $T^{\tilde{\pi}_n}$, and the triangle
622 inequality, and (b) follows from both T^* and $T^{\tilde{\pi}_n}$ (for a fixed π_n) are contractions. This together
623 with Lemma 2 implies that

$$\|Q^* - Q^{\tilde{\pi}_n}\|_\infty \leq \frac{2\gamma\|Q^* - Q_n\|_\infty + \Delta}{1 - \gamma} \quad (6)$$

624 We then bound $\|Q^* - Q_n\|_\infty$ as follows

$$\|Q^* - Q_{n+1}\|_\infty \leq \|T^*Q^* - T^*Q_n\|_\infty + \|T^*Q_n - Q_{n+1}\|_\infty \leq \gamma\|Q^* - Q_n\|_\infty + \Delta,$$

625 which implies that

$$\limsup_{n \rightarrow \infty} \|Q^* - Q_n\|_\infty \leq \frac{\Delta}{1 - \gamma} \quad (7)$$

626 Plug this back in equation 6, we have

$$\limsup_{n \rightarrow \infty} \|Q^* - Q^{\tilde{\pi}_n}\|_\infty \leq \frac{1 + \gamma}{(1 - \gamma)^2} \Delta \quad (8)$$

627 where $\Delta = 2\epsilon\gamma(l_r + l_p|S|\frac{R_{max}}{1-\gamma})$. □

628 E.2 A counterexample to $T^{\pi_n \circ \omega_{\pi_n}}$ being a contraction when $\pi_n \circ \omega_{\pi_n}$ is not fixed

629 Consider an MDP $\langle S, A, P, R, \gamma \rangle$ where $S = \{s_1, s_2, s_3\}$ and $A = \{a_1, a_2, a_3\}$. Suppose that for any
630 $s \in S$ and $a \in A$, $P(s_2|s, a) = 1$ and $P(s'|s, a) = 0$ for $s' \neq s_2$, and $B_\epsilon(s) = \{s_1, s_2, s_3\}$. Con-
631 sider the two Q -functions shown in Table 2. We have $\|Q_1 - Q_2\|_\infty = |Q_1(s_2, a_2) - Q_2(s_2, a_2)| = 10$.
632 However, when $\tilde{\pi}_1 = \pi_1 \circ \omega_{\pi_1}$ is derived from Q_1 and $\tilde{\pi}_2 = \pi_2 \circ \omega_{\pi_2}$ is derived from Q_2 ,

$$\begin{aligned} \|T^{\tilde{\pi}_1}Q_1 - T^{\tilde{\pi}_2}Q_2\|_\infty &= \max_{s \in S, a \in A, s' \in S} \sum \gamma P(s'|s, a) |Q_1(s', \pi_1(\omega_{\pi_1}(s'))) - Q_2(s', \pi_2(\omega_{\pi_2}(s')))| \\ &= \max_{s \in S, a \in A} \gamma |Q_1(s_2, \pi_1(\omega_{\pi_1}(s'))) - Q_2(s, \pi_2(\omega_{\pi_2}(s')))| \\ &\geq \gamma |Q_1(s_2, \pi_1(\omega_{\pi_1}(s_2))) - Q_2(s_2, \pi_2(\omega_{\pi_2}(s_2)))| \\ &\stackrel{(a)}{=} \gamma |Q_1(s_2, a_1) - Q_2(s_2, a_2)| \\ &= \gamma \times 11 \\ &\stackrel{(b)}{>} 10 = \|Q_1 - Q_2\|_\infty \end{aligned}$$

633 where (a) is due to the fact that no matter what $\omega_\pi(s_2)$ is, $B_\epsilon(\omega_\pi(s_2)) = \{s_1, s_2, s_3\} = S$, which
634 implies that $\pi_1(\omega_{\pi_1}(s_2)) = \operatorname{argmax}_{a \in A} \min_{\bar{s} \in S} Q_1(\bar{s}, a) = a_1$, and similarly, $\pi_2(\omega_{\pi_2}(s_2)) = a_2$;
635 (b) holds when $\gamma > \frac{10}{11}$. Therefore, $T^{\pi_1 \circ \omega_{\pi_1}}$ is not a contraction.

636 **F Algorithms**

Algorithm 2: Belief Update

Data: Old Belief M_t , action a , perturbed state \tilde{s}_{t+1} .

Result: Updated Belief M_{t+1}

```

1 Initialize  $M'_t$  to be an empty set
2 for  $s$  in  $M_t$  do
3   for  $s'$  in  $S$  do
637 4     if  $P(s'|s, a) \neq 0$  then
5       |   Add  $s'$  to  $M'_t$ 
6       |   end
7     end
8 end
9  $M_{t+1} = M'_t \cap B_\epsilon(\tilde{s}_{t+1})$ 
10 RETURN  $M_{t+1}$ 

```

Algorithm 3: Pessimistic Q-Iteration

Result: Robust Q-function Q

```

1 Initialize  $Q_0(s, a) = 0$  for all  $s \in S, a \in A$ ;
2 for  $n = 0, 1, 2, \dots$  do
3   Update RL agent policy:  $\forall \tilde{s} \in S, \pi_n(\tilde{s}) = \operatorname{argmax}_{a \in A} \min_{\bar{s} \in B_\epsilon(\tilde{s})} Q_n(\bar{s}, a)$ ;
4   Update attacker policy:  $\forall s \in S, \omega_{\pi_n}(s) = \operatorname{argmin}_{\tilde{s} \in B_\epsilon(s)} Q_n(s, \pi_n(\tilde{s}))$ ;
638 5   for  $s \in S$  do
6     |   for  $a \in A$  do
7     |   |    $Q_{n+1}(s, a) = R(s, a) + \gamma \sum_{s' \in S} P(s'|s, a) Q_n(s', \pi(\omega_{\pi_n}(s)))$ ;
8     |   end
9   end
10 end

```

Algorithm 4: Belief-Enriched Pessimistic DQN (BP-DQN) Training. We highlight the difference between our algorithm and the vanilla DQN algorithm in **brown**.

Data: Number of iterations T , trained vanilla Q network Q_v , PF-RNN belief model N_p , target network update frequency Z , batch size D , exploration parameter ϵ'

Result: Robust Q network Q_r

```

1 Initialize replay buffer  $\mathcal{B}$ , robust Q network  $Q_r = Q_v$ , target Q network  $Q' = Q_v$ , observation
  history  $S_{his}$ , action history  $A_{his}$ ;
2 for  $t = 0, 1, \dots, T$  do
3   Use PGD to find the best perturb state  $\tilde{s}_t$  that minimizes  $Q_r(s_t, \pi(\tilde{s}_t))$ , where  $\pi$  is derived
  from  $Q_r$  by taking greedy action;
4    $M_t = M_t \cap B_\epsilon(\tilde{s}_t)$ ;
5   Choose an action based on belief  $M_t$  and  $Q_r$  using  $\epsilon$ -greedy:
   $a_t = \operatorname{argmax}_{a \in A} \min_{m \in M_t} Q_r(m, a)$  with probability  $1 - \epsilon'$ ; otherwise  $a_t$  is a random
639 6   action;
7   Append  $\tilde{s}_t$  and  $a_t$  to  $S_{his}$  and  $A_{his}$  and use belief model  $N_p(S_{his}, A_{his})$  to generate  $M_{t+1}$ ;
8   Execute action  $a_t$  in the environment and observe reward  $R_t$  and next true state  $s_{t+1}$ ;
9   if  $s_{t+1}$  is a terminal state then
10    |   Reset  $S_{his}$  and  $A_{his}$ 
11    end
12    Store transition  $\{s_t, a_t, R_t, s_{t+1}, M_t\}$  in  $\mathcal{B}$ ;
13    Sample a random minibatch of size  $D$  of transitions  $\{s_i, a_i, R_i, s_{i+1}, M_i\}$  from  $\mathcal{B}$ ;
14    Set  $y_i = \begin{cases} R_i & \text{for terminal } s_{i+1} \\ R_i + \gamma \max_{a' \in A} \min_{m \in M_i} Q'(m, a') & \text{for non-terminal } s_{i+1} \end{cases}$ ;
15    Perform a gradient descent step to minimize  $\text{Huber}(\sum_i y_i - Q_r(s_i, a_i))$ ;
16    Update target network every  $Z$  steps;
17 end

```

Algorithm 5: Belief-Enriched Pessimistic DQN (BP-DQN) Testing

Data: Trained robust Q network Q_r , PFRNN belief model N_p

```
1 Initialize observation history  $S_{his}$  and action history  $A_{his}$ ;  
2 for  $t = 0, 1, \dots, T$  do  
3   Observe the perturbed state  $\tilde{s}_t$ ;  
4   if  $t = 0$  then  
640      $M_0 = B_\epsilon(\tilde{s}_t)$ ;  
6   end  
7   Select an action based on belief  $M_t$  and  $Q_r$ :  $a_t = \operatorname{argmax}_{a \in A} \min_{m \in M_t} Q_r(m, a)$ ;  
8   Append  $\tilde{s}_t$  and  $a_t$  to  $S_{his}$  and  $A_{his}$  and use belief model  $N_p(S_{his}, A_{his})$  to generate  $M_{t+1}$ ;  
9   Execute action  $a_t$  in the environment;  
10 end
```

Algorithm 6: Diffusion-Assisted Pessimistic DQN (DP-DQN) Training. We highlight the difference between our algorithm and the vanilla DQN algorithm in **brown**.

Data: Number of iterations T , trained vanilla Q network Q_v , diffusion belief model N_d , target network update frequency Z , batch size D , belief size κ_d , exploration parameter ϵ' , noise level ϵ_ϕ **Result:** Robust Q network Q_r

```
1 Initialize replay buffer  $\mathcal{B}$ , robust Q network  $Q_r = Q_v$ , target Q network  $Q' = Q_v$ ;  
2 for  $t = 0, 1, \dots, T$  do  
3   Use PGD to find the best perturb state  $\tilde{s}_t$  that minimizes  $Q_r(s_t, \pi(\tilde{s}_t))$ , where  $\pi$  is derived  
   from  $Q_r$  by taking greedy action;  
4   Sample noise  $\phi$  uniformly from  $(-\epsilon_\phi, \epsilon_\phi)$  with same dimension as  $s_t$  pixel-wise;  
5   Use the diffusion belief model to generate belief  $M_t = N_d(\tilde{s}_t + \phi)$  of size  $\kappa_d$ ;  
641 6   Select an actions based on belief  $M_t$  and  $Q_r$  using  $\epsilon$ -greedy:  
    $a_t = \operatorname{argmax}_{a \in A} \min_{m \in M_t} Q_r(m, a)$  with probability  $1 - \epsilon'$ ; otherwise  $a_t$  is a random  
   action;  
7   Execute action  $a_t$  in environment and observe reward  $R_t$  and next true state  $s_{t+1}$ ;  
8   Apply the reverse diffusion process to  $s_t$  and  $s_{t+1}$ :  $\hat{s}_t = N_d(s_t)$ ,  $\hat{s}_{t+1} = N_d(s_{t+1})$ ;  
9   Store transition  $\{\hat{s}_t, a_t, R_t, \hat{s}_{t+1}, M_t\}$  in  $\mathcal{B}$ ;  
10  Sample a random minibatch of size  $D$  of transitions  $\{\hat{s}_i, a_i, R_i, \hat{s}_{i+1}, M_i\}$  from  $\mathcal{B}$ ;  
11  Set  $y_i = \begin{cases} R_i & \text{for terminal } \hat{s}_{i+1} \\ R_i + \gamma \max_{a' \in A} \min_{m \in M_i} Q'(m, a') & \text{for non-terminal } \hat{s}_{i+1} \end{cases}$   
12  Perform a gradient descent step to minimize  $\text{Huber}(\sum_i y_i - Q_r(\hat{s}_i, a_i))$ ;  
13  Update target network every  $Z$  steps;  
14 end
```

Algorithm 7: Diffusion-Assisted Pessimistic DQN (DP-DQN) Testing

Data: Trained robust Q network Q_r , diffusion belief model N_d , noise level ϵ_ϕ

```
1 for  $t = 0, 1, \dots, T$  do  
2   Observe the perturbed state  $\tilde{s}_t$ ;  
642 3   Sample noise  $\phi$  uniformly from  $(-\epsilon_\phi, \epsilon_\phi)$  with same dimension as  $s_t$  pixel-wise;  
4   Generate belief using the diffusion belief model  $M_t = N_d(\tilde{s}_t + \phi)$ ;  
5   Choose an action based on belief  $M_t$  and  $Q_r$ :  $a_t = \operatorname{argmax}_{a \in A} \min_{m \in M_t} Q_r(m, a)$ ;  
6   Execute action  $a_t$  in the environment;  
7 end
```

643 G Experiment Details and Additional Results

644 G.1 Experiment Setup Justification

645 Although both the BP-DQN and DP-DQN algorithms follow our idea of pessimistic Q-learning, the
646 former is more appropriate for games with a discrete or a continuous but low-dimensional state space

647 such as the continuous Gridworld environment, while the latter is more appropriate for games with
648 raw pixel input such as Atari Games.

649 In the Gridworld environment, state perturbations can manipulate the semantics of states by changing
650 the coordinates of the agent. In this case, historical information can be utilized to generate beliefs
651 about true states. Following this idea, BP-DQN uses the particle filter recurrent neural network (PF-
652 RNN) method to predict true states. In principle, we can also use BP-DQN on the Atari environments
653 to predict true states through historical data. In practice, however, it is computationally challenging
654 to do so due to the high-dimensional state space (84×84) of the Atari environments. Developing
655 more efficient belief update techniques for large environments remains an active research direction.

656 On the other hand, state perturbations are injected pixel-wise in state-of-the-art attacks in Atari
657 games. Consequently, they can barely change the semantics of true states Atari environments. In
658 this case, historical information becomes less useful, and the diffusion model can effectively “purify”
659 the perturbed states to recover the true states from high-dimensional image data. Although it is
660 theoretically possible to use DP-DQN on the Gridworld environment, we conjecture that it is less
661 effective than BP-DQN since it does not utilize historical data, which is crucial to recover true states
662 when perturbations can change the semantic meaning of states as in the case of continuous Gridworld.
663 In particular, we observe that the distributions of perturbed states and true states are very similar in
664 this environment, making it difficult to learn a diffusion model that can map the perturbed states back
665 to true states.

666 It is an interesting direction to develop strong perturbation attacks that can manipulate the semantics
667 of true states for games with raw pixel input. As a countermeasure, we can potentially integrate
668 diffusion-based state purification and belief-based history modeling to craft a stronger defense.

669 G.2 Experiment Setup

670 **Environments.** The continuous state Gridworld is modified from the grid maze environment in [21].
671 We create a 10×10 map with walls inside. There are also gold and a bomb in the environment where
672 the agent aims to find the gold and avoid the bomb. The state space is a tuple of two real numbers in
673 $[0, 10] \times [0, 10]$ representing the coordinate of the agent. The initial state of the agent is randomized.
674 The agent can move in 8 directions, which are up, up left, left, down left, down, down right, right, and
675 up right. By taking an action, the agent moves a distance of 0.5 units in the direction they choose. For
676 example, if the agent is currently positioned at (x, y) and chooses to move upwards, the next state
677 will be $(x, y + 0.5)$. If the agent chooses to move diagonally to the upper right, the next state will
678 be $(x + 0.5/\sqrt{2}, y + 0.5/\sqrt{2})$. If the agent would collide with a wall by taking an action, it remains
679 stationary at its current location during that step. The agent loses 1 point for each time step before the
680 game ends and gains a reward of 200 points for reaching the gold and -50 points for reaching the
681 bomb. The game terminates once the agent reaches the gold or bomb or spends 100 steps in the game.
682 For Atari games, we choose Pong and Freeway provided by the OpenAI Gym [4].

683 **Baselines.** We choose vanilla DQN [23], SA-DQN [33] and WocaR-DQN [20] as defense baselines.
684 We consider three commonly used attacks to evaluate the robustness of these algorithms: (1) PGD
685 attack [33], which aims to find a perturbed state \tilde{s} that minimizes $Q(s, \pi(\tilde{s}))$ and we set PGD steps
686 $\eta = 10$ for both training and testing usage; (2) MinBest attack [14], which aims to find a perturbed
687 state \tilde{s} that minimizes the probability of choosing the best action under s , with the probabilities of
688 actions represented by a softmax of Q-values; and (3) PA-AD [27], which utilizes RL to find a (nearly)
689 optimal attack policy. For each attack, we choose $\epsilon \in \{0.1, 0.5\}$ for the Gridworld environment and
690 $\epsilon \in \{1/255, 3/255, 15/255\}$ for the Atari games. Natural rewards (without attacks) are reported
691 using policies trained under $\epsilon = 0.1$ for continuous state Gridworld and $\epsilon = 1/255$ for Atari games.

692 **Training and Testing Details.** We use the same network structure as vanilla DQN [23], which is
693 also used in SA-DQN [33] and WocaR-DQN [20]. We set all parameters as default in their papers
694 when training both SA-DQN and WocaR-DQN. For training our pessimistic DQN algorithm with
695 PF-RNN-based belief (called BP-DQN, see Algorithm 4 in Appendix F), we set $\kappa_p = |M_t| = 30$, i.e.,
696 the PF-RNN model will generate 30 belief states in each time step. For training our pessimistic DQN
697 algorithm with diffusion (called DP-DQN, see Algorithm 6 in Appendix F), we set $\kappa_d = |M_t| = 4$,
698 that is, the diffusion model generates 4 purified belief states from a perturbed state. We consider two
699 variants of DP-DQN, namely, DP-DQN-O and DP-DQN-F, which utilize DDPM and Progressive
700 Distillation as the diffusion model, respectively. For DP-DQN-O, we set the number of reverse steps

| Env | Parameter | PGD | | | MinBest | | | PA-AD | | |
|---------|-----------------------------|--------------------|--------------------|---------------------|--------------------|--------------------|---------------------|--------------------|--------------------|---------------------|
| | | $\epsilon = 1/255$ | $\epsilon = 3/255$ | $\epsilon = 15/255$ | $\epsilon = 1/255$ | $\epsilon = 3/255$ | $\epsilon = 15/255$ | $\epsilon = 1/255$ | $\epsilon = 3/255$ | $\epsilon = 15/255$ |
| Pong | noise level ϵ_ϕ | 2/255 | 15/255 | 8/255 | 18/255 | 15/255 | 8/255 | 15/255 | 15/255 | 8/255 |
| | reverse step k | 1 | 1 | 1 | 1 | 1 | 1 | 4 | 4 | 4 |
| | sampler step | 64 | 32 | 32 | 32 | 32 | 32 | 64 | 64 | 64 |
| Freeway | noise level ϵ_ϕ | 5/255 | 5/255 | 5/255 | 5/255 | 5/255 | 5/255 | 5/255 | 5/255 | 5/255 |
| | reverse step k | 1 | 4 | 4 | 1 | 4 | 4 | 2 | 4 | 4 |
| | sampler step | 64 | 64 | 64 | 64 | 64 | 64 | 64 | 64 | 64 |

Table 3: Parameters Used to Test DP-DQN-F

701 to $k = 10$ for $\epsilon = 1/255$ or $3/255$ and $k = 30$ for $\epsilon = 15/255$, and do not add noise ϕ when training
702 and testing DP-DQN-O. For DP-DQN-F, we set $k = 1$, sampler step to 64, and add random noise
703 with $\epsilon_\phi = 5/255$ when training DP-DQN-F. We report the parameters used when testing DP-DQN-F
704 in Table 3. We sample $C = C' = 30$ trajectories to train PF-RNN and diffusion models. All other
705 parameters are set as default for training the PF-RNN and diffusion models. For all other baselines,
706 we train 1 million frames for the continuous Gridworld environment and 6 million frames for the
707 Atari games. For our methods, we take the pre-trained vanilla DQN model, and train our method
708 for another 1 million frames. All training and testing are done on a machine equipped with an
709 i9-12900KF CPU and a single RTX 3090 GPU. For each environment, all RL policies are tested in
710 10 randomized environments with means and variances reported.

711 G.3 More Experiment Results

712 G.3.1 More Baseline Results

713 Tables 4a and 4b give the complete results for the continuous space Gridworld and the two Atari
714 games, where we include another baseline called Radial-DQN [24], which adds an adversarial loss
715 term to the nominal loss of regular DRL in order to gain robustness. We find that Radial-DQN fails to
716 learn a reasonable policy in continuous Gridworld as other regularization-based methods. However,
717 Radial-DQN performs well under a small attack budget in Atari games but still fails to respond when
718 the attack budget is high. Our Radial-DQN results for the Atari games were obtained using the
pre-trained models [24], which might explain why the results are better than those reported in [20].

| Environment | Model | Natural Reward | PGD | | MinBest | |
|----------------------|---------------|------------------|------------------|------------------|------------------|------------------|
| | | | $\epsilon = 0.1$ | $\epsilon = 0.5$ | $\epsilon = 0.1$ | $\epsilon = 0.5$ |
| Continuous Gridworld | DQN | 156.5 \pm 90.2 | 128 \pm 118 | -53 \pm 86 | 98.2 \pm 137 | 98.2 \pm 137 |
| | SA-DQN | 20.8 \pm 140 | 46 \pm 142 | -100 \pm 0 | -5.8 \pm 131 | -100 \pm 0 |
| | WocaR-DQN | -100 \pm 0 | -100 \pm 0 | -63.2 \pm 88 | -100 \pm 0 | -63.2 \pm 88 |
| | Radial-DQN | -100 \pm 0 | -96.1 \pm 12.3 | -96.1 \pm 12.3 | -100 \pm 0 | -100 \pm 0 |
| | BP-DQN (Ours) | 163 \pm 26 | 165 \pm 29 | 176 \pm 16 | 147 \pm 88 | 114 \pm 114 |

(a) Continuous Gridworld Results

| Env | Model | Natural Reward | PGD | | | MinBest | | | PA-AD | | |
|---------|----------------|----------------|--------------------|--------------------|---------------------|--------------------|--------------------|---------------------|--------------------|--------------------|---------------------|
| | | | $\epsilon = 1/255$ | $\epsilon = 3/255$ | $\epsilon = 15/255$ | $\epsilon = 1/255$ | $\epsilon = 3/255$ | $\epsilon = 15/255$ | $\epsilon = 1/255$ | $\epsilon = 3/255$ | $\epsilon = 15/255$ |
| Pong | DQN | 21 \pm 0 | -21 \pm 0 | -21 \pm 0 | -21 \pm 0 | -21 \pm 0 | -21 \pm 0 | -21 \pm 0 | -21 \pm 0 | -21 \pm 0 | |
| | SA-DQN | 21 \pm 0 | 21 \pm 0 | 21 \pm 0 | -20.8 \pm 0.4 | 21 \pm 0 | 21 \pm 0 | -21 \pm 0 | 21 \pm 0 | 18.7 \pm 2.6 | -20 \pm 0 |
| | WocaR-DQN | 21 \pm 0 | 21 \pm 0 | 21 \pm 0 | -21 \pm 0 | 21 \pm 0 | 21 \pm 0 | -21 \pm 0 | 21 \pm 0 | 19.7 \pm 2.4 | -21 \pm 0 |
| | Radial-DQN | 21 \pm 0 | 21 \pm 0 | 21 \pm 0 | -21 \pm 0 | 21 \pm 0 | 21 \pm 0 | -21 \pm 0 | 21 \pm 0 | 21 \pm 0 | -19 \pm 0 |
| | DP-DQN-O(Ours) | 19.9 \pm 0.3 | 19.8 \pm 0.4 | 19.7 \pm 0.5 | 19.9 \pm 0.3 | 19.9 \pm 0.3 | 19.3 \pm 0.8 | 19.9 \pm 0.3 | 19.9 \pm 0.3 | 19.3 \pm 0.8 | 19.3 \pm 0.8 |
| | DP-DQN-F(Ours) | 21 \pm 0 | 20.4 \pm 0.7 | 20.2 \pm 0.8 | 18.6 \pm 1 | 20.2 \pm 0.9 | 19.0 \pm 0 | 19.3 \pm 1.6 | 18.0 \pm 1.0 | 17.6 \pm 1.8 | 17 \pm 2.3 |
| Freeway | DQN | 34 \pm 0.1 | 0 \pm 0 | 0 \pm 0 | 0 \pm 0 | 0 \pm 0 | 0 \pm 0 | 0 \pm 0 | 0 \pm 0 | 0 \pm 0 | |
| | SA-DQN | 30 \pm 0 | 30 \pm 0 | 30 \pm 0 | 0 \pm 0 | 27.2 \pm 3.4 | 18.3 \pm 3.0 | 0 \pm 0 | 20.1 \pm 4.0 | 9.5 \pm 3.8 | 0 \pm 0 |
| | WocaR-DQN | 31.2 \pm 0.4 | 31.2 \pm 0.5 | 31.4 \pm 0.3 | 21.6 \pm 1 | 29.6 \pm 2.5 | 19.8 \pm 3.8 | 21.6 \pm 1 | 24.9 \pm 3.7 | 12.3 \pm 3.2 | 21.6 \pm 1 |
| | Radial-DQN | 33.4 \pm 0.5 | 33.4 \pm 0.5 | 33.4 \pm 0.5 | 21.6 \pm 1 | 33.4 \pm 0.5 | 32.8 \pm 0.8 | 21.6 \pm 1 | 33.4 \pm 0.5 | 33.4 \pm 0.5 | 21.6 \pm 1 |
| | DP-DQN-O(Ours) | 28.8 \pm 1.1 | 29.1 \pm 1.1 | 29 \pm 0.9 | 28.9 \pm 0.7 | 29.2 \pm 1.0 | 28.5 \pm 1.2 | 28.6 \pm 1.3 | 28.6 \pm 1.2 | 28.3 \pm 1 | 28.8 \pm 1.1 |
| | DP-DQN-F(Ours) | 31.2 \pm 1 | 30 \pm 0.9 | 30.1 \pm 1 | 30.7 \pm 1.2 | 30.2 \pm 1.3 | 30.6 \pm 1.4 | 29.4 \pm 1.2 | 30.8 \pm 1 | 31.4 \pm 0/8 | 28.9 \pm 1.1 |

(b) Atari Games Results

Table 4: Experiment Results. We show the average episode rewards \pm standard deviation over 10 episodes for our methods and three baselines. The results for our methods are highlighted in gray.

719

720 G.3.2 More Ablation Study Results

721 **Importance of Combining Maximin and Belief.** In Table 5a, we compare our methods (BP-DQN
722 and DP-DQN-O) that integrate the ideas of maximin search and belief approximation (using either

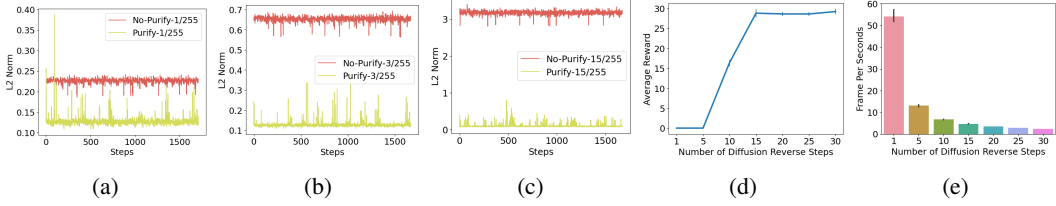


Figure 5: a), b) and c) show the l_2 distance between perturbed states and original states before and after purification under different attack budgets in the Pong environment using DDPM. d) shows the performance of DP-DQN-O under different diffusion steps in the Freeway environment under PGD attack with $\epsilon = 15/255$. e) shows the testing stage speed of DP-DQN-O (measured by the number of frames processed per second) under different diffusion steps in the Freeway environment.

| Environment | Model | PGD | Environment | Model | PA-AD |
|----------------------|---------------|------------------|-------------|-----------------|---------------------|
| | | $\epsilon = 0.5$ | | | $\epsilon = 15/255$ |
| Continuous Gridworld | Maximin Only | -71 ± 91 | Pong | Maximin Only | -21 ± 0 |
| | Belief Only | 45.7 ± 134 | | DDPM Only | 18.8 ± 1.6 |
| | BP-DQN (Ours) | 176 ± 16 | | DP-DQN-O (Ours) | 19.3 ± 0.8 |

(a) Ablation Study Results. We compare our methods with variants that use maximin search or belief approximation only.

| Environment | Model | Training (hours) | Testing (FPS) | Environment | Model | Training (hours) | Testing (FPS) |
|----------------------|--------------|------------------|-----------------|-------------|-----------------|------------------|---------------|
| GridWorld Continuous | SA-DQN | 3 | 607 | Pong | SA-DQN | 38 | 502 |
| | WocaR-DQN | 3.5 | 721 | | WocaR-DQN | 50 | 635 |
| | BP-DQN(Ours) | 0.6+1.5+7 | 192 | | DP-DQN-O (Ours) | 1.5+18+30 | 6.6 |
| | | | DP-DQN-F (Ours) | | 1+18+24 | 93 | |

(b) Training and Testing Time Comparison. The training of our methods contains three parts: a) training the PF-RNN or diffusion model, b) training a vanilla DQN policy without attacks, and c) training a robust policy using BP-DQN, DP-DQN-O, or DP-DQN-F.

Table 5: Ablation and Time Comparison Results

RNN or diffusion) with variants of our methods that use maximin search or belief approximation only. The former is implemented using a trained BP-DQN or DP-DQN-O policy together with random samples from the ϵ -ball centered at a perturbed state (the worst-case belief) during the test stage. The latter uses the vanilla DQN policy with a single belief state generated by either the PF-RNN or the DDPM diffusion model at the test stage. The results clearly demonstrate the importance of integrating both ideas to achieve more robust defenses.

Diffusion Effects. In Figures 5a-5c, we visualize the effect of DDPM-based diffusion by recording the l_2 distance between a true state and the perturbed state and that between a purified true state and the purified perturbed state. For all three levels of attack budgets, our diffusion model successfully shrinks the gap between true states and perturbed states.

Performance vs. Running Time in DP-DQN. We study the impact of different diffusion steps k on average return of DP-DQN-O in Figure 5d and their testing stage running time in Figure 5e. Figure 5d shows the performance under different diffusion steps of our method in the Freeway environment under PGD attack with budget $\epsilon = 15/255$. It shows that we need enough diffusion steps to gain good robustness, and more diffusion steps do not harm the return but do incur extra overhead, as shown in Figure 5e, where we plot the testing stage running time in Frame Per Second (FPS). As the number of diffusion steps increases, the running time of our method also increases, as expected.

On the other hand, as DP-DQN-F uses a distilled sampler, it can decrease the reverse sample step k to as small as 1, which greatly reduces the testing time as reported in Table ???. We report the performance results of DP-DQN-F in Table 1b and we find that DP-DQN-F improves DP-DQN-O under small perturbations, but suffers performance loss in Pong under PA-AD attack and large perturbations. Further, DP-DQN-F has a larger standard deviation than DP-DQN in the Pong environment, indicating that DP-DQN-F is less stable than DP-DQN-O in Pong. We conjecture that the lower sample quality introduced by Progressive Distillation causes less stable performance and performance loss under PA-AD attack compared to DP-DQN-O that utilizes DDPM.

748 **Training and Testing Overhead.** Table 5b compares the training and test-stage overhead of SA-
749 DQN, WocaR-DQN, and our methods. Notice that the training of our methods consists of three parts:
750 a) training the PF-RNN belief model or the diffusion model, b) training a vanilla DQN policy without
751 attacks, and c) training a robust policy using BP-DQN, DP-DQN-O or DP-DQN-F. In the continuous
752 state Gridworld environment, our method takes around 9 hours to finish training, which is higher than
753 SA-DQN and WocaR-DQN. But our method significantly outperforms these two baselines as shown
754 in Table 1a. In the Atari Pong game, our method takes about 50 hours to train, which is comparable
755 to WocaR-DQN but slower than SA-DQN. In terms of running time at the test stage, we calculate the
756 FPS of each method and report the average FPS over 5 testing episodes. In the continuous Gridworld
757 environment, our method is slower but comparable to SA-DQN and WocaR-DQN due to the belief
758 update and maximin search. However, in the Atari Pong game, our DP-DQN-O method is much
759 slower than both SA-DQN and WocaR-DQN. This is mainly due to the use of a large diffusion model
760 in our method. However, our DP-DQN-F method is around 13 times faster than DP-DQN-O and is
761 comparable to SA-DQN and WocaR-DQN.

762 H Conclusion and Limitations

763 In conclusion, this work proposes two algorithms, BP-DQN and DP-DQN, to combat state per-
764 turbations against reinforcement learning. Our methods achieve high robustness and significantly
765 outperform state-of-the-art baselines under strong attacks. Further, our DP-DQN method has revealed
766 an important limitation of existing state adversarial attacks on RL agents with raw pixel input, pointing
767 to a promising direction for future research.

768 However, our work also has some limitations. First, our method needs access to a clean environment
769 during training. Although the same assumption has been made in most previous work in this area,
770 including SA-MDP and WocaR-MDP, a promising direction is to consider an offline setting to release
771 the need to access a clean environment by learning directly from (possibly poisoned) trajectory data.
772 Second, using a diffusion model increases the computational complexity of our method and causes
773 slow running speed at the test stage. Fortunately, we have shown that fast diffusion methods can
774 significantly speed up runtime performance. Third, we have focused on value-based methods in this
775 work. Extending our approach to policy-based methods is an important next step.